J. Fluid Mech. (2007), *vol.* 592, *pp.* 335–366. © 2007 Cambridge University Press
doi:10.1017/S0022112007008531 Printed in the United Kingdom

Small-scale statistics in high-resolution direct numerical simulation of turbulence: Reynolds number dependence of one-point velocity gradient statistics

T. ISHIHARA[1]†, Y. KANEDA[1], M. YOKOKAWA[2], K. ITAKURA[3] AND A. UNO[2]

[1]Department of Computational Science and Engineering, Graduate school of Engineering, Nagoya University, Chikusa-ku, Nagoya 464-8603, Japan

[2]Next-Generation Supercomputer R&D Center RIKEN, 2-1-1 Marunouchi, Chiyoda-ku, Tokyo 100-0005, Japan

[3]Super Computer System Planning and Operations Department, Japan Agency for Marine–Earth Science and Technology, 3173-25 Showa-machi, Kanazawa-ku, Yokohama 236-0001, Japan

(Received 6 January 2007 and in revised form 1 August 2007)

One-point statistics of velocity gradients and Eulerian and Lagrangian accelerations are studied by analysing the data from high-resolution direct numerical simulations (DNS) of turbulence in a periodic box, with up to 4096^3 grid points. The DNS consist of two series of runs; one is with $k_{\max}\eta \sim 1$ (Series 1) and the other is with $k_{\max}\eta \sim 2$ (Series 2), where $k_{\max}$ is the maximum wavenumber and η the Kolmogorov length scale. The maximum Taylor-microscale Reynolds number R_λ in Series 1 is about 1130, and it is about 675 in Series 2. Particular attention is paid to the possible Reynolds number (Re) dependence of the statistics. The visualization of the intense vorticity regions shows that the turbulence field at high Re consists of clusters of small intense vorticity regions, and their structure is to be distinguished from those of small eddies. The possible dependence on Re of the probability distribution functions of velocity gradients is analysed through the dependence on R_λ of the skewness and flatness factors (S and F). The DNS data suggest that the R_λ dependence of S and F of the longitudinal velocity gradients fit well with a simple power law: $S \sim -0.32{R_\lambda}^{0.11}$ and $F \sim 1.14{R_\lambda}^{0.34}$, in fairly good agreement with previous experimental data. They also suggest that all the fourth-order moments of velocity gradients scale with R_λ similarly to each other at $R_\lambda > 100$, in contrast to $R_\lambda < 100$. Regarding the statistics of time derivatives, the second-order time derivatives of turbulent velocities are more intermittent than the first-order ones for both the Eulerian and Lagrangian velocities, and the Lagrangian time derivatives of turbulent velocities are more intermittent than the Eulerian time derivatives, as would be expected. The flatness factor of the Lagrangian acceleration is as large as 90 at $R_\lambda \approx 430$. The flatness factors of the Eulerian and Lagrangian accelerations increase with R_λ approximately proportional to ${R_\lambda}^{\alpha_E}$ and ${R_\lambda}^{\alpha_L}$, respectively, where $\alpha_E \approx 0.5$ and $\alpha_L \approx 1.0$, while those of the second-order time derivatives of the Eulerian and Lagrangian velocities increases approximately proportional to ${R_\lambda}^{\beta_E}$ and ${R_\lambda}^{\beta_L}$, respectively, where $\beta_E \approx 1.5$ and $\beta_L \approx 3.0$.

† Author to whom correspondence should be addressed: ishihara@cse.nagoya-u.ac.jp.

1. Introduction

Because of recent rapid developments in computational facilities and methods, computational approaches are of increasing importance in the study of turbulence, as in many other fields of science and technology. Among these approaches are those based on direct numerical simulation (DNS) of turbulence, which can provide us with detailed and accurate data of turbulence under well-controlled conditions. DNS can be useful not only for practical applications, but also for the understanding of the fundamental features of turbulence, especially the possible universality in the small-scale statistics of turbulence at high Reynolds number, the exploration of which is one of the most important challenges in modern turbulence study.

There have been extensive studies of turbulence based on DNS of incompressible turbulence under simple boundary conditions. Simple boundary conditions, such as periodic ones, reduce computational costs, and their use is consistent with the idea of Kolmogorov (1941, hereafter K41), according to which the small-scale statistics are insensitive to the details of the forcing and boundary conditions at large scales. The resolution level in the DNS has been increasing rapidly with the developments in supercomputing technology (e.g. see Ishihara & Kaneda 2002).

It should be recalled here, however, that the number of degrees of freedom (DOF) increases rapidly with the Reynolds number, Re, and the DOF which can be treated in the DNS is limited by the available computer memory and speed; thus the resolution or Re achievable in DNS has until now been severely limited. On the other hand, even if a universality of turbulence at small scales in the sense of K41 is true, it can be realized only at sufficiently high Re. If Re is low, the flow may be sensitive to the forcing and boundary conditions at large scales, and it is very unlikely to show the universal features of turbulence at high Re. For example, in DNS with the number of grid points, $N \leqslant 512$ or 1024, the width of the inertial subrange may still be too narrow, as demonstrated by Ishihara & Kaneda (2002). Moreover, it is difficult to know *a priori* how large Re must be to detect the universality. Some features of turbulence observed at low or moderate Re may no longer be observed at high Re. Little is known about the quantitative aspects of the Re dependence on the turbulence statistics at high Re.

These considerations motivate us to perform DNS with Re as high as possible to obtain some idea of the Re dependence on the statistics, or its approach to universality in the asymptotic limit of $Re \to \infty$. Fortunately, we could perform high-resolution DNS of incompressible turbulence on the Earth Simulator (at Japan Agency for Marine–Earth Science and Technology) with up to 4096^3 grid points, which is 64 times larger than the 1024^3 in the largest previous DNS.

In this paper, we focus our attention on the one-point statistics of velocity gradients in homogeneous isotropic turbulence. The statistics are dominated by small-scale statistics of turbulence. If the small-scale statistics are universal in the sense of K41, the universality must be exhibited in the statistics of the gradients. In this sense, the statistics may be regarded as among the most fundamental statistics of turbulence, and has attracted extensive studies by experiments as well as by DNS. Among these statistics are the skewness S and flatness factor F of velocity gradients, studied especially by experiments (e.g. see Tabeling *et al.* 1996; Sreenivasan & Antonia 1997; Gylfason, Ayyalasomayajula & Warhaft 2004 and the references cited therein). Not only have S and F been studied by DNS and experiments, but so have the other higher-order moments of velocity derivatives (e.g. see Siggia 1981*a*; Kerr 1985; Belin *et al.* 1997; Zhou & Antonia 2000).

These studies raise several questions, among them the following.

(*a*) Is $|S|$ a monotonically increasing function of Re? Experimental studies suggest that $|S|$ is an increasing function of Re for large Re, but DNS so far suggest that S tends to be a constant for large Re.

(*b*) Is there any transition of the Re dependence of F? Tabeling *et al.* (1996) suggested experimentally that there may be a transition of the Re dependence of F at $R_\lambda \approx 700$, but Gylfason *et al.* (2004) argued on the basis of their experiments that there is no such transition.

(*c*) Do all the four rotational invariants of velocity gradients, in terms of which all fourth-order moments of velocity gradients in homogeneous isotropic turbulence can be expressed (Siggia 1981*b*; Hiero & Dopazo 2003), scale with Re similarly to each other at high Re? By analysing his DNS data, Kerr (1985) argued that they scale differently from each other. However, R_λ was only up to approximately 83. Can one extrapolate the result to higher R_λ?

The intermittency of turbulence occurs not only in space, but also in time; thus it is seen not only in the velocity gradients, but also in the time derivatives of turbulent velocities. In this paper, we therefore study not only the one-point statistics of velocity gradients, but also those of the Eulerian and Lagrangian accelerations and related quantities, such as pressure gradients. Extensive studies have been made of these statistics (e.g. see Gotoh & Rogallo 1999; Yeung 2002 and references cited therein, e.g. Vedula & Yeung 1999; Gotoh & Fukayama 2001; La Porta *et al.* 2001, and Hill 2002*a*; Sawford *et al.* 2003; Biferale *et al.* 2004; Biferale *et al.* 2005; Yeung *et al.* 2006).

The purpose of this paper is to extend the studies of one-point statistics to higher Re as a result of our high-resolution DNS data. Particular attention is paid to the possible Re dependence of the statistics. It is hoped that the analysis presented in this paper may provide a basis for further exploration of the universality of small-scale statistics of turbulence, as well as for developing turbulence theories or models at high Re.

This paper is organized as follows. Section 2 presents the DNS method, and § 3 shows the run conditions and turbulence characteristics. Section 4 is devoted to one-point statistics of the velocity gradients and the related statistics, and § 5 to the statistics of the Eulerian and Lagrangian accelerations and their time derivatives. Section 6 presents an analysis of the statistics from the viewpoint of spectral decomposition. Discussions are given in § 7, and § 8 provides the conclusions.

2. Method of simulation

We consider three-dimensional turbulence of incompressible fluid of unit density that obeys the Navier–Stokes (NS) equation

$$\frac{\partial}{\partial t}\boldsymbol{u} + (\boldsymbol{u}\cdot\nabla)\boldsymbol{u} = -\nabla p + \nu\Delta\boldsymbol{u} + \boldsymbol{f}, \tag{2.1}$$

with the continuity equation

$$\nabla\cdot\boldsymbol{u} = 0. \tag{2.2}$$

Here $\boldsymbol{u}$, p, ν and $\boldsymbol{f}$ denote velocity, pressure, kinematic viscosity and external force, respectively. The turbulence field is assumed to be periodic in each direction of the Cartesian coordinates with a fundamental periodic box of size 2π, so that it can be expressed as a Fourier series with both the minimum wavenumber $k_{\min}$ and the wavenumber increment being 1.

The NS equations are solved by a fully alias-free spectral method, where aliasing errors are removed by the so-called phase-shift method, and we can keep all the Fourier modes satisfying $k < k_{\max} \equiv \sqrt{2}N/3$, where k is the wavenumber and N the number of grid points in each of the Cartesian coordinates in real space. The time marching of the DNS is performed by a fourth-order Runge–Kutta method.

To maintain a statistically quasi-stationary state of turbulence, we need to force the field. For this purpose, we may take as the force field a white noise in time. However, introducing randomness externally may mix the intrinsic randomness because of the inherent NS dynamics with external randomness, and it is quite unlikely that the characteristic time of the external force at a large scale is as short as white noise. We therefore chose to force the field in a deterministic way, as was done by Kerr (1985), Vincent & Meneguzzi (1991) and Jiménez *et al.* (1993). The forcing is given by $\hat{\boldsymbol{f}}(\boldsymbol{k}) = -c\hat{\boldsymbol{u}}(\boldsymbol{k})$ in the wavevector space, where $\hat{\boldsymbol{f}}$ and $\hat{\boldsymbol{u}}$ are Fourier transforms of $\boldsymbol{f}$ and $\boldsymbol{u}$, respectively. The value of c is set at non-zero only in the wavenumber range $k < K_c$ and is adjusted at every time step so as to keep the total kinematic energy E almost time independent (≈ 0.5). In the runs reported below, we set $K_c = 2.5$. The forcing is confined to a low wavenumber range so that it does not directly affect the dynamics at the small scales.

In all the runs reported below, except those with $N = 4096$, we used double-precision arithmetic. The sustained performance of 16.4 Tflops was achieved in a DNS with $N = 2048$ on the Earth Simulator. Further details of parallel computing on the Earth Simulator are given in Yokokawa *et al.* (2002). In the runs with $N = 4096$, we also used double-precision arithmetic for the evaluation of the nonlinear convolution sums in the wavevector space, but we used single-precision arithmetic for the linear viscous term and time marching to save the machine memory. Preliminary DNS with $N = 1024$ showed the effect of reducing the precision to be insignificant, at least for low-order statistics such as the energy spectrum (see Yokokawa *et al.* 2002; Kaneda *et al.* 2003).

Prior to carrying out DNS with $N \geqslant 512$, we had performed them with $N = 256$ by using a random initial field. The runs were continued until a certain time $t = t_F$. We then started new runs (i) reducing the kinematic viscosity ν, (ii) doubling N and (iii) using the final state of the run with the smaller N as the initial state of the new runs, and we continued the runs until a certain final time $t = t_F$. A similar process was repeated for larger N.

The statistics from the DNS may depend on the maximum wavenumber $k_{\max}$ retained in the DNS. Previous studies suggest that it is desirable to take $k_{\max}\eta > 1$, where η is the Kolmogorov dissipation length scale defined by $\eta = (\nu^3/\langle\epsilon\rangle)^{1/4}$ (Jiménez *et al.* 1993; Yamazaki, Ishihara & Kaneda 2002). A comparison of DNS with different resolutions, with $k_{\max}\eta = 0.5$, 1.0 and 2.0, suggests that although the solution trajectories in the phase space are sensitive to the resolution level, as would be expected, the low-order statistics are insensitive to the resolution (Yamazaki *et al.* 2002). To get some idea of the possible dependence of the statistics on $k_{\max}$, we performed two series of DNS, Series 1 and Series 2, for which $k_{\max}\eta \approx 1$ and $k_{\max}\eta \approx 2$, respectively. For comparison, we also performed a DNS with $N = 512$, $k_{\max}\eta \approx 4$, where the final state of Run 256-2 was used as the initial state. We use these data in the following.

3. Run conditions and global turbulence characteristics

Table 1 summarizes some key values characterizing the runs, in which the instantaneous mean energy dissipation rate $\langle\epsilon\rangle$ and the integral length scale L are

Run	N	$10^{-3}Re$	R_λ	$k_{\max}$	$10^3\Delta t$	$10^4\nu$	$\langle\epsilon\rangle$	L	λ	$10^3\eta$	T	τ_η	t_F
256-1	256	0.936	167	121	1.0	7.00	0.0849	1.13	0.203	7.97	1.96	0.091	10
512-1	512	2.10	257	241	1.0	2.8	0.0902	1.02	0.125	3.95	1.77	0.056	10
1024-1	1024	6.71	471	483	0.625	1.1	0.0683	1.28	0.0897	2.10	2.21	0.040	10
2048-1	2048	16.1	732	965	0.4	0.44	0.0707	1.23	0.0558	1.05	2.13	0.025	10
4096-1	4096	36.5	1131	1930	0.25	0.173	0.0752	1.09	0.0339	0.51	1.89	0.015	4.525
256-2	256	0.318	94	121	1.0	20	0.0936	1.10	0.327	17.1	1.91	0.147	10
512-2	512	1.00	173	241	1.0	7.0	0.0795	1.21	0.210	8.10	2.10	0.094	10
1024-2	1024	2.31	268	483	0.625	2.8	0.0829	1.12	0.130	4.03	1.94	0.058	10
2048-2	2048	5.31	429	965	0.4	1.1	0.0824	1.01	0.0817	2.00	1.75	0.037	10
4096-2	4096	13.7	675	1930	0.25	0.44	0.0831	1.05	0.0515	1.01	1.82	0.023	3.8
512-4	512	0.323	95	241	1.0	20	0.0931	1.12	0.328	17.1	1.94	0.146	2

TABLE 1. DNS parameters and turbulence characteristics at the final time $t = t_F$.

computed in terms of the three-dimensional energy spectrum $E(k)$, as

$$\langle\epsilon\rangle = 2\nu \int_0^{k_{\max}} k^2 E(k)\,\mathrm{d}k, \quad L = \frac{\pi}{2u'^2} \int_0^{k_{\max}} k^{-1} E(k)\,\mathrm{d}k,$$

where $\frac{3}{2}u'^2$ is the total kinetic energy $E = \int E(k)\,\mathrm{d}k$. The Reynolds number Re is defined as $Re = u'L/\nu$. The Taylor microscale λ and the microscale Reynolds number R_λ are given by $\lambda = (15\nu u'^2/\langle\epsilon\rangle)^{1/2}$ and $R_\lambda = u'\lambda/\nu$, respectively, and the eddy turnover time T and the Kolmogorov dissipation time scale τ_η are given by $T = L/u'$ and $\tau_\eta = (\nu/\langle\epsilon\rangle)^{1/2}$, respectively.

In table 1, $\Delta t/\tau_\eta \approx 0.02$ in Series 1 and $\Delta t/\tau_\eta \approx 0.01$ in Series 2, except for Run 256-1 and Run 256-2. In terms of $T_C \equiv \Delta x/u'$ ($\approx 2\pi\sqrt{3}/N$ in our runs), Δt is in the range $0.02 < \Delta t/T_C < 0.1$. For example, in Run 4096-1 (4096-2), $\Delta t/\tau_\eta \approx 0.016$ (0.011) and $\Delta t/T_C \approx 0.094$ (0.094). Note that $\tau_\eta/T = 15^{1/2}\alpha^{-1}R_\lambda^{-1}$, $T_C/T = 15^{3/4}C\alpha^{-1}R_\lambda^{-3/2}$ and $T_C/\tau_\eta = 15^{1/4}CR_\lambda^{-1/2}$, where $\alpha \equiv \langle\epsilon\rangle L/u'^3$, $C \equiv \Delta x/\eta$ and $\Delta x/\eta \approx 2\sqrt{2}\pi/3$ and $\sqrt{2}\pi/3$ in Series 1 and 2, respectively.

3.1. *Time dependence of global statistics*

Although the total kinetic energy E is kept almost time independent (≈ 0.5) in our DNS, the turbulence statistics are not stationary in a strict sense. To examine the possible time dependence of the statistics, we monitored the time dependence of representative statistics during the DNS, some of which are shown in figure 1.

Figures 1(*a*) and 1(*b*) show the time dependence of $\langle\epsilon\rangle$ and R_λ, respectively. It is seen in figure 1(*a*) that in each run, $\langle\epsilon\rangle$ increases rapidly at the initial stage, and then after reaching a peak, say at time $t = t_P$, decreases to a local minimum, say at time $t = t_L$. After that, its time dependence is rather weak. The times t_P and t_L are smaller for the larger Reynolds number. This suggests that the transient time period is shorter for the larger Reynolds number. This is also the case for R_λ in figure 1(*b*). These results are consistent with a study by Ishihara & Kaneda (2002) on the time dependence of various turbulence statistics for DNS with N up to 1024. Figure 1 presents an extension of the study for DNS with N up to 4096.

The DNS data give

$$t_P \approx 30\tau_\eta, \quad \text{i.e.} \quad t_P \approx 7.7\lambda/u' \propto T/R_\lambda, \tag{3.1}$$

except Run 256-1 and Run 256-2, which are started from a random initial field. The estimate (3.1) implies that the transient time during which the dissipation range

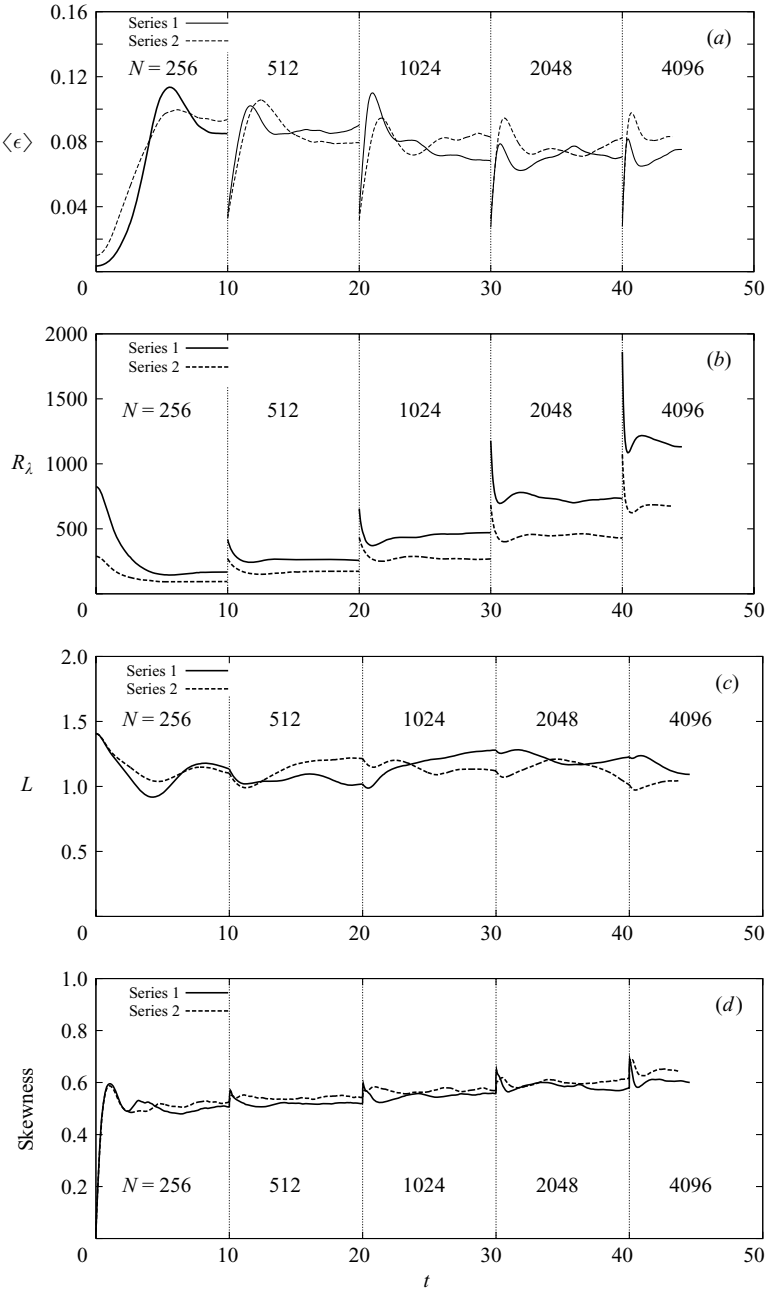

FIGURE 1. (*a*) Mean energy dissipation rate $\langle\epsilon\rangle$, (*b*) Taylor-microscale Reynolds number R_λ, (*c*) integral length scale L and (*d*) skewness of the longitudinal velocity derivative, vs. time t, for Series 1 (solid lines) and Series 2 (dashed lines). The values of ν and N were changed at $t = 10$, 20, 30 and 40.

structure readjusts to the sudden decrease of ν is proportional to τ_η, and it decreases with R_λ in proportion to R_λ^{-1}, for given T.

Figure 1(*c*) shows the time dependence of the integral length scale L. Since u' is almost fixed in our DNS, λ, R_λ and η are determined by $\langle\epsilon\rangle$, and the eddy turnover

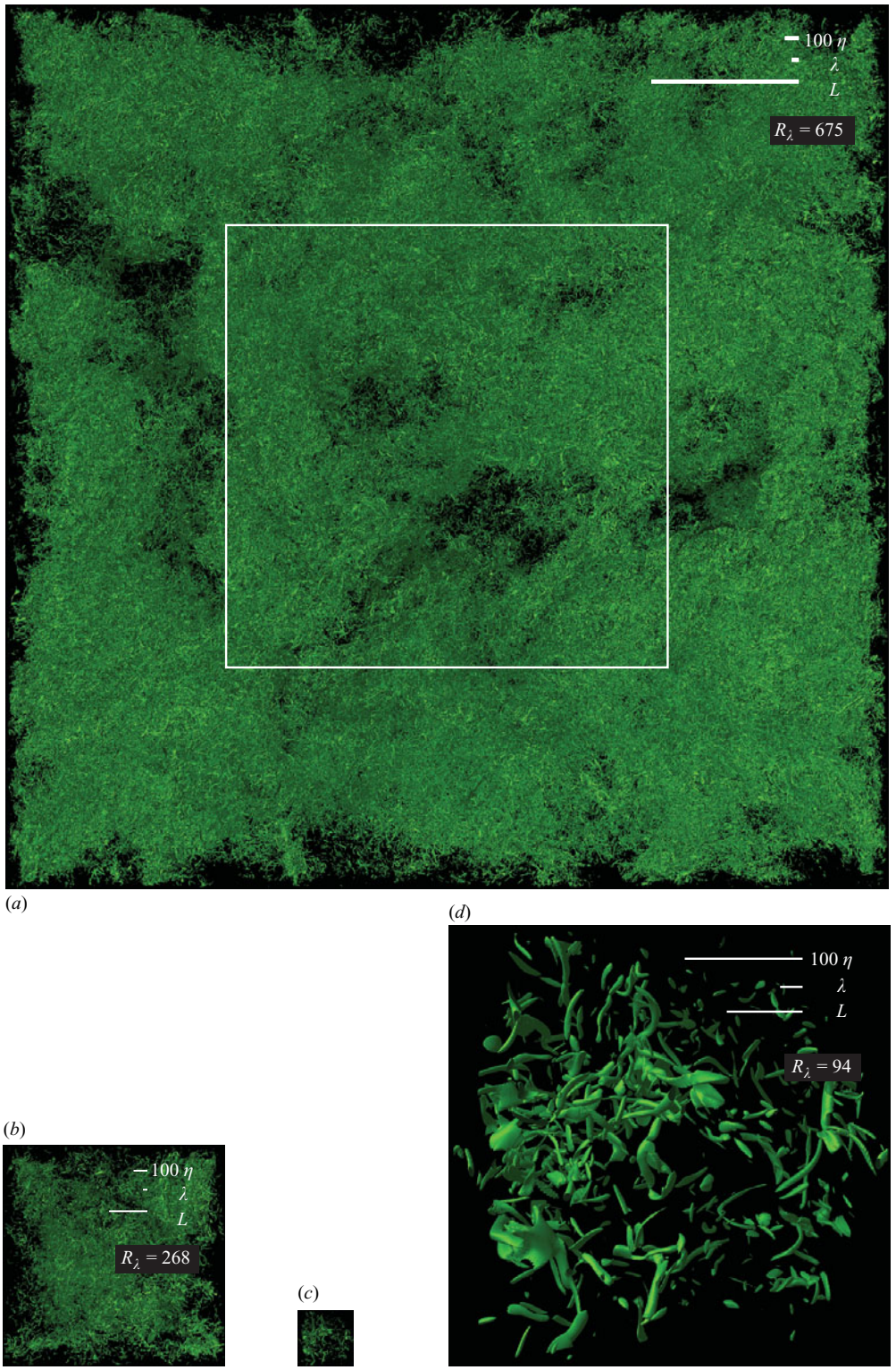

FIGURE 2. (*a*) Equivorticity surface showing the intense vorticity regions with $|\boldsymbol{\omega}| > \bar{\omega} + 4\sigma$ in Run 4096-2, where ω is the vorticity and ω and σ are the mean and the standard deviation of ω, respectively. The straight lines on the upper right corner show the lengths 100η, λ, and L. (*b*) and (*c*) Intense vorticity regions in Run 1024-2 and Run 256-2, respectively. The frame size of (*a*)–(*c*) is proportional to N. (*d*) Enlargement of (*c*).

time $T \equiv L/u'$ and Re by L. In contrast to $\langle\epsilon\rangle$ and R_λ, no sharp initial change is seen in figure 1(c) for L. Throughout, L is approximately 1.0–1.3. Since $u' \approx 1/\sqrt{3}$ and $L \approx 1.15$ in the runs, the eddy turnover time $T = L/u'$ is approximately 2; thus $t/T \approx t/2$.

Figure 1(d) shows the time dependence of the skewness factor of the longitudinal velocity derivative defined by

$$S \equiv \frac{\left\langle (\partial u/\partial x)^3 \right\rangle}{\left\langle (\partial u/\partial x)^2 \right\rangle^{3/2}}. \tag{3.2}$$

Because of the randomness of the initial field, $S \approx 0$ at $t = 0$ in the starting runs with $N = 256$. The skewness S increases rapidly in an initial transient period, then reaches a state where the time dependence is not as strong. The time dependence of S is not strong in the other runs with $N \geqslant 512$. Figure 1(d) shows that S is larger for the larger Reynolds number (see § 4.2).

These results suggest that after a certain initial transient stage, which is shorter for the larger Reynolds number in our DNS, the non-stationarity of the statistics is weak. If we are interested in (quasi-) stationary statistics, rather than those in the transient phase, we need to continue the runs at least until the time t_{L} of the local minimum of $\langle\epsilon\rangle$. In the following, we present the statistics of the final field at $t = t_{\mathrm{F}} (> t_{\mathrm{L}})$ of each run, unless otherwise stated.

3.2. *Visualization*

The amount of data generated by simulations on an advanced supercomputer such as the Earth Simulator is generally huge, and it is often difficult to extract an intuitive understanding. A visualization may therefore provide an overview of the simulated field before a detailed quantitative analysis of the data.

Figure 2(a) gives an example of such a visualization. It shows the intense vorticity regions in Run 4096-2 ($R_\lambda = 675$). The displayed domain size is $(4096\Delta)^2 \times 2048\Delta$, where $V = (4096\Delta)^3$ is the total volume of the fundamental periodic domain. For comparison, the intense-vorticity regions in DNS with lower resolutions, $N = 1024$ and 256, in Series 2 are also plotted in figures 2(b) and 2(c), respectively. Each figure also shows the integral length scale L, the Taylor microlength scale λ and the Kolmogorov length scale η. The frame size of figure 2(a–c) is proportional to N. Figure 2(d) is an enlargement of figure 2(c), and figures 3(a) to 3(d) shows increasingly close-up views of figure 2(a).

The ratios L/η and λ/η are seen to be larger for the larger Reynolds number, in agreement with Kaneda & Ishihara (2006), which confirmed that the DNS data fit quite well with the scaling derived by a simple dimensional analysis based on Kolmogorov's idea:

$$N \sim C_1 Re^{3/4}, \quad R_\lambda \sim C_2 Re^{1/2},$$
$$L/\eta \sim C_3 Re^{3/4}, \quad \lambda/\eta \sim C_4 Re^{1/4},$$

where $Re \equiv u'L/\nu$, and C_1 is a constant that depends on $k_{\max}\eta$. According to Kolmogorov, C_2, C_3, and C_4 are universal constants at high Re. Table 1 gives $C_1 \approx 1.5$ in Series 1, and $C_1 \approx 3.2$ in Series 2 and

$$C_2 \approx 6.0, \quad C_3 \approx 0.81, \quad C_4 \approx 4.8$$

in both Series 1 and 2.

A visualization of turbulence fields by DNS with low resolution or low Reynolds number, such as that in figure 2(*d*), from DNS with $N = 256$ and $R_\lambda = 94$, might give an impression that the turbulence field is dominated by a not so large number of strong vortices, some of which may span the whole simulation domain. We might then hope that the turbulence field may be well described by a dynamic system with a small number of degrees of freedom representing the dynamics of strong vortices. However, figure 2(*a*) and figures 3(*a*) to 3(*d*) suggest that this is not so at high Reynolds number. The turbulence field at high *Re* consists of a huge number of small vortices. They form clusters, and void regions are seen at various scales. The structure of the clusters is different from that of the worms. It is very unlikely that such a system could be represented as a dynamic system with a small number of degrees of freedom. It is also unlikely that the statistics of the fine-scale structures of high-*Re* turbulence are the same as those of low-*Re* turbulence.

These observations suggest the importance of not confusing statistics at low *Re* and high *Re*. In the following, we analyse the small-scale statistics of turbulence while taking into account the possible *Re* dependence of the statistics.

4. One-point statistics of velocity gradients

4.1. *Probability distribution functions*

The intermittency of turbulence on a small scale is manifested in the velocity gradients. Figure 4 shows the velocity gradients, (*a*) $\partial u/\partial x$ and (*b*) $\partial v/\partial x$, and two components of vorticity, (*c*) ω_x and (*d*) ω_y, along a line in the direction of x at various R_λ. It provides us with an intuitive idea of the increase of intermittency with the Reynolds number. The figures suggest that the intermittencies of these quantities are qualitatively not very different from each other.

An intermittency, such as that in figure 4, may be quantified in terms of probability distribution functions (p.d.f.) or histograms. Figures 5(*a*) and 5(*b*) show p.d.f.'s of the longitudinal velocity gradient $\partial u/\partial x$ for Series 1 and 2, respectively. If they were Gaussian, the curves would be parabolic in figure 5. The figures show that they are far from Gaussian. They have wide tails, which are wider for larger R_λ. Similar R_λ trends have been reported for lower R_λ (e.g. see Jiménez *et al.* 1993; Gotoh, Fukayama & Nakano 2002). The figures also suggest that the curves do not converge to a single curve with the increase of R_λ, at least in the range of R_λ studied here. The same is also true for the p.d.f.'s of the transversal velocity gradient $\partial v/\partial x$ and vorticity component ω_x, as respectively seen in figures 5(*c*) and 5(*d*). Figure 5(*e*) shows that the normalized p.d.f. of ω_x is almost identical to that of $\partial v/\partial x$ and that the tails of the p.d.f.'s for ω_x and $\partial v/\partial x$ are wider than for $\partial u/\partial x$, and ω_x and $\partial v/\partial x$ are more intermittent than $\partial u/\partial x$.

A close inspection of the figures reveals that wavenumber truncation, such as $k_{\max}\eta = 1$ or $k_{\max}\eta = 2$, may affect the p.d.f.'s. To see this point more clearly, we plotted the p.d.f.'s of $\partial u/\partial x$ at similar values of R_λ, from Series 1 and 2 in figure 5(*f*). It is seen that the tail of the p.d.f. in Run 2048-2 ($R_\lambda = 429$) is wider than that in Run 1024-1 ($R_\lambda = 471$), in spite of R_λ in the former being smaller. A similar trend has also been reported for lower R_λ in Jiménez *et al.* (1993). This suggests that p.d.f.'s for very large $|\partial u/\partial x|$ or $|\partial v/\partial x|$ in Series 1 ($k_{\max}\eta = 1$) are underestimated in comparison with those in Series 2 ($k_{\max}\eta = 2$). This is presumably because the small-scale eddies with very high k or high velocity gradients are less well resolved in DNS in Series 1 than in Series 2, as is expected when viewed in terms of spectral cutoff filters of different filter widths. (For the effect of wavenumber truncation, see also the discussion in § 4.4.)

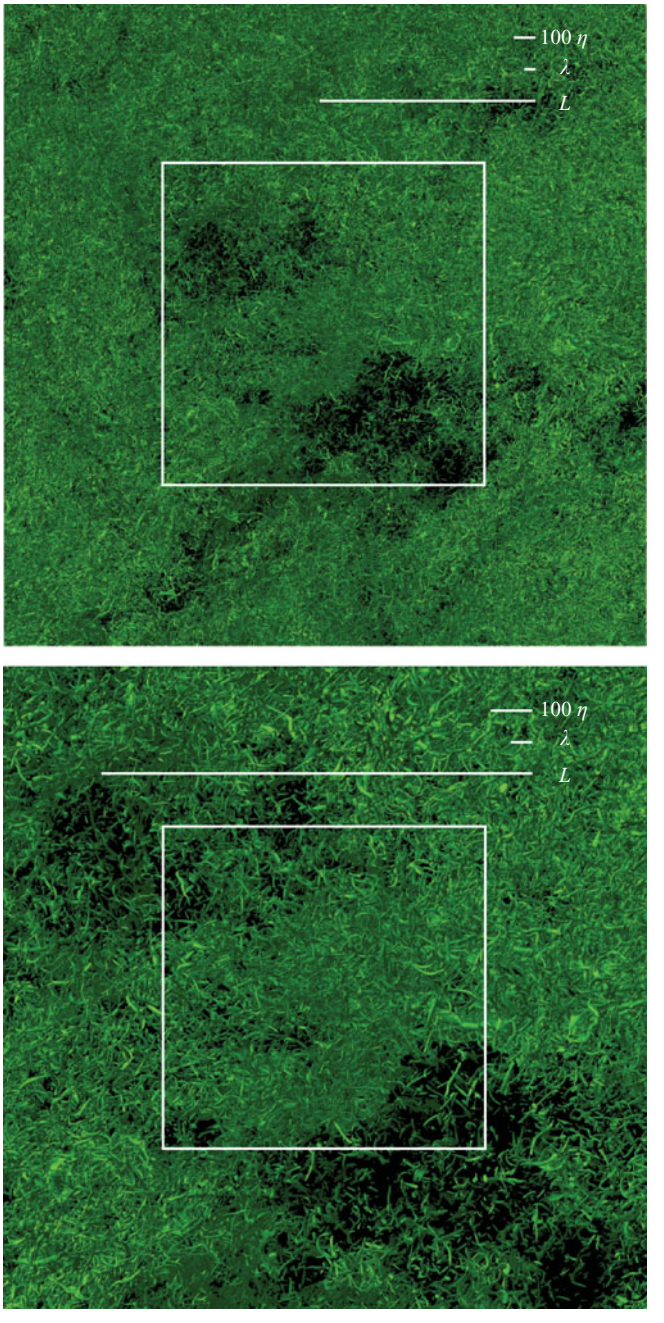

FIGURE 3(*a*, *b*). For caption see facing page.

4.2. *Skewness of the longitudinal velocity gradient*

Moments of the velocity gradients provide us with simple measures characterizing the non-Gaussianity and the possible R_λ dependence of the p.d.f.'s. Among such moments are the third-order moment or skewness S of the longitudinal velocity derivative $\partial u/\partial x$ defined by (3.2). It is zero if the p.d.f. is Gaussian. In homogenous isotropic turbulence, any third-order moment of the velocity gradient tensor $g_{ij} = (\partial u_i/\partial x_j)$ can be expressed in terms of the skewness S defined by (3.2) (Champagne 1978). In

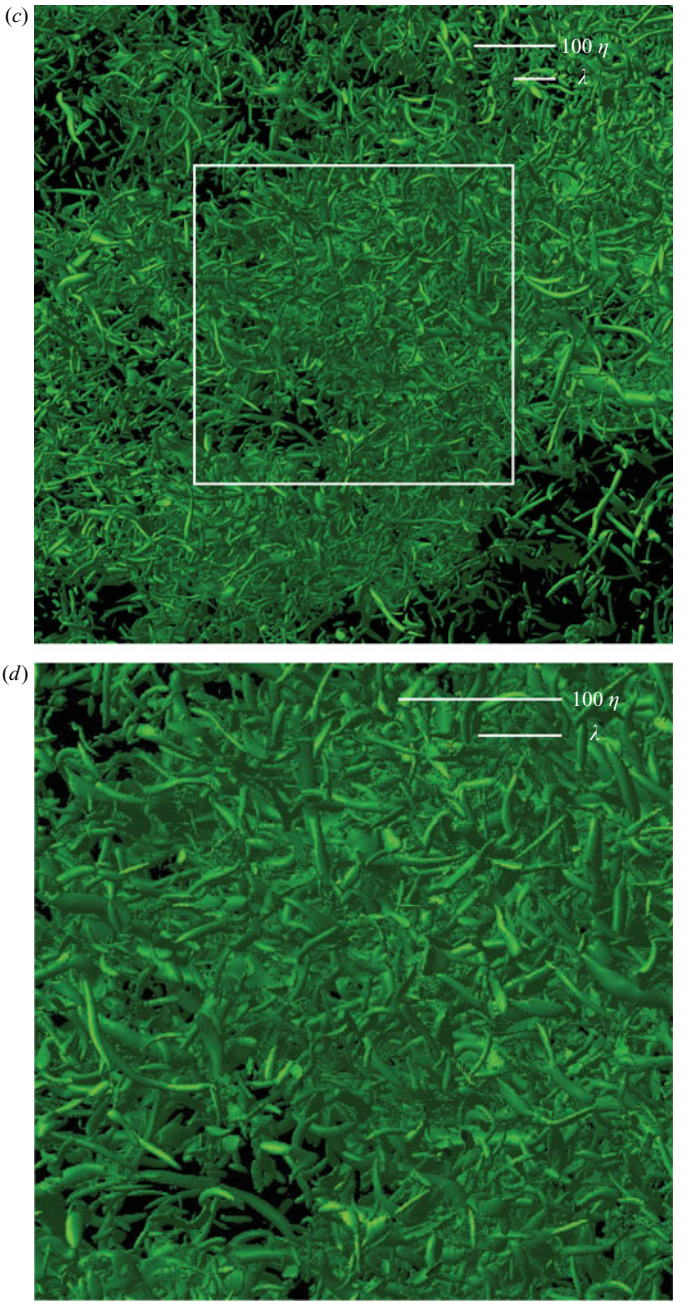

FIGURE 3. (*a*) A closer view of the inner region of figure 2(*a*). (*b*) A closer view of the inner region of (*a*). (*c*) A closer view of the inner region of (*b*). (*d*) A closer view of the inner region of (*c*).

such turbulence, S may also be computed by

$$S = -\frac{2}{35}\frac{\int k^2 T(k)\,\mathrm{d}k}{\left(\langle\epsilon\rangle/15\nu\right)^{3/2}}, \tag{4.1}$$

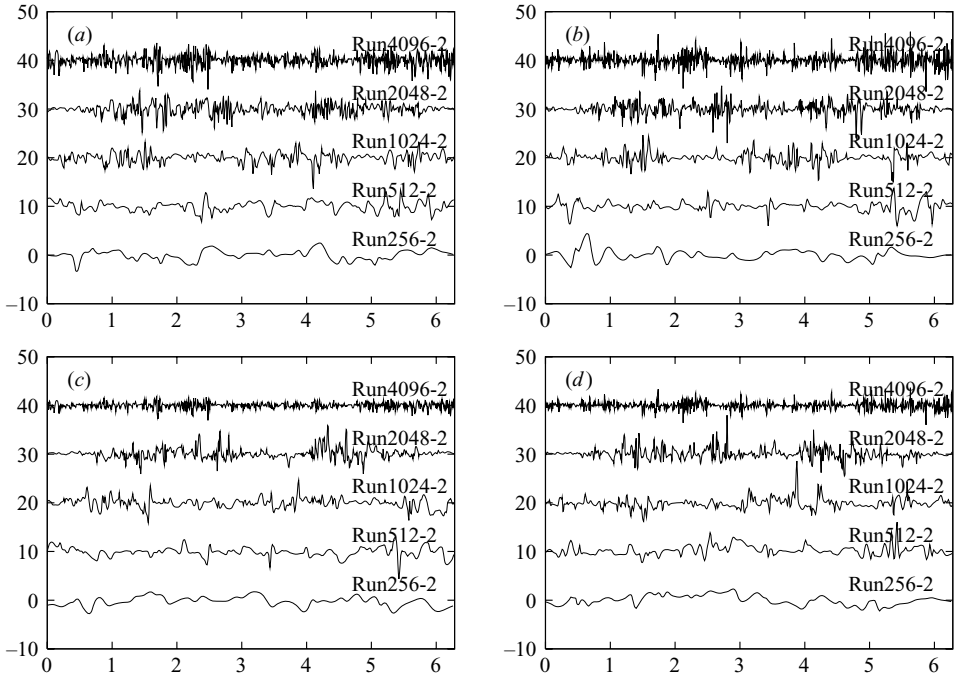

FIGURE 4. Normalized velocity gradients (*a*) $\partial u/\partial x$ and (*b*) $\partial v/\partial x$, and vorticity components (*c*) ω_x and (*d*) ω_y, along the line $y = z = 0$, for Run 256-2, Run 512-2, Run 1024-2, Run 2048-2 and Run 4096-2. The normalization is based on standard deviations. The curves for Run 512-2, Run 1024-2, Run 2048-2 and Run 4096-2 are shifted upward by 10, 20, 30 and 40, respectively.

because

$$\langle \epsilon \rangle = 15\nu \left\langle (\partial u/\partial x)^2 \right\rangle \text{ and } \left\langle (\partial u/\partial x)^3 \right\rangle = -\frac{2}{35} \int k^2 T(k)\, \mathrm{d}k,$$

where $T(k)$ is the energy transfer function given by

$$T(k) = 2\pi k^2 [\langle \hat{\boldsymbol{N}}(\boldsymbol{k}) \cdot \hat{\boldsymbol{u}}(-\boldsymbol{k}) \rangle + \langle \hat{\boldsymbol{N}}(-\boldsymbol{k}) \cdot \hat{\boldsymbol{u}}(\boldsymbol{k}) \rangle]$$

and $\hat{\boldsymbol{N}}(\boldsymbol{k})$ is the Fourier transform of $-(\boldsymbol{u} \cdot \nabla)\boldsymbol{u}$ under an appropriate normalization. We have confirmed that the value of S computed by (3.2) is almost identical to that computed by (4.1).

Figure 6 plots the values of S in the present DNS, where time averages taken in Series 2 are also plotted (the implication of the time average will be discussed in § 7.1). The DNS and experimental data from figure 5 in Sreenivasan & Antonia (1997) and the DNS data from Wang *et al.* (1996) and Gotoh *et al.* (2002) are also included in the figure.

If only the data for $R_\lambda < 200$ were available, S would tend to a constant independent of R_λ with the increase of R_λ. However, the data for larger $R_\lambda (>200)$ show that S has a weak dependence on R_λ at larger R_λ. Thus figure 6 presents an example that the statistics at low $R_\lambda (<200)$ cannot be extrapolated to higher $R_\lambda (>200)$.

On the basis of the data at $R_\lambda > 400$ of Antonia, Chambers & Satyaprakash (1981), Hill (2002*a*) proposed

$$-S \sim 0.5(R_\lambda/400)^{0.11} \left(\sim 0.26 {R_\lambda}^{0.11}\right), \tag{4.2}$$

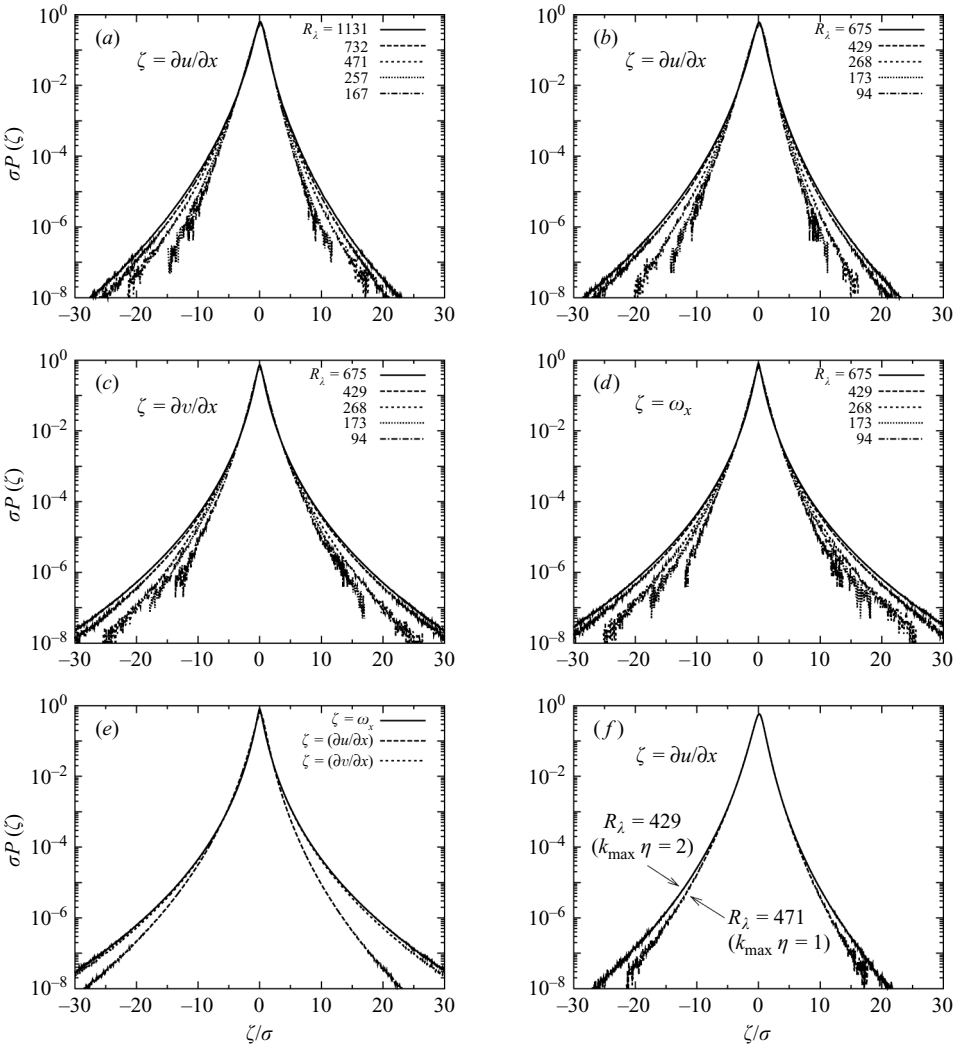

FIGURE 5. The p.d.f.'s of ζ for (*a*) $\zeta = \partial u/\partial x$ in Series 1, (*b*) $\zeta = \partial u/\partial x$ in Series 2, (*c*) $\zeta = \partial v/\partial x$ in Series 2 and (*d*) $\zeta = \omega_x$ in Series 2. (*e*) The p.d.f.'s for $\zeta = \omega_x$, $\zeta = \partial u/\partial x$ and $\zeta = \partial v/\partial x$ in Run 2048-2. (*f*) A comparison of p.d.f.'s for $\zeta = \partial v/\partial x$ in Run 1024-1 with $R_\lambda = 471$ (dashed line) and in Run 2048-2 with $R_\lambda = 429$ (solid line). σ is the standard deviation of ζ in each p.d.f.

and Gylfason *et al.* (2004) showed that

$$-S \sim 0.33 R_\lambda^{0.09}. \tag{4.3}$$

fitted well their experimental data.

Our DNS values of $-S$ for $R_\lambda > 200$, especially those in Series 1, agree well with (4.3). However, a close inspection shows also that the DNS values of $-S$ in Series 2 are larger than those in Series 1, and they are slightly larger than (4.2) and (4.3). A least-square fitting of the data of Series 2 to $\ln(-S) \sim \alpha + \beta \ln R_\lambda$ yields

$$-S \sim (0.32 \mp 0.02) R_\lambda^{0.11 \pm 0.01}, \tag{4.4}$$

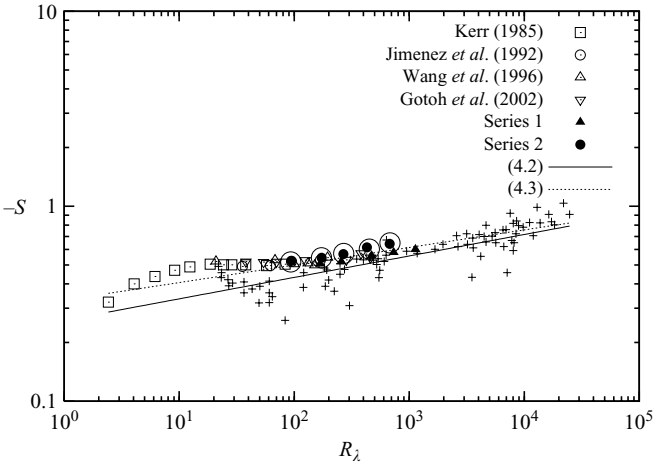

FIGURE 6. Skewness S of the longitudinal velocity gradient $\partial u/\partial x$ vs. R_λ. The filled triangles (▲) and circles (●) are the values at $t = t_F$ in Series 1 and 2, respectively; the large circles denote the time averages of $(R_\lambda, -S)$ over t from $t = t_F/2$ to t_F in each run of Series 2. The symbols □, ○, + are from figure 5 in Sreenivasan & Antonia (1997), △ from Wang *et al.* (1996), and ▽ from Gotoh *et al.* (2002); the crosses (+) are from experiments, while the others are from DNS.

instead of (4.2) and (4.3); we confirmed that the fitting of the time-averaged data instead of the instantaneous data leads to no significant changes in the result.

4.3. *Flatness factor of the longitudinal velocity gradient*

The non-Gaussianity or the intermittency and the possible R_λ dependence of the p.d.f.'s may be characterized quantitatively not only by the skewness, but also by the flatness factor defined as

$$F \equiv \frac{\langle (\partial u/\partial x)^4 \rangle}{\langle (\partial u/\partial x)^2 \rangle^2},$$

which is equal to $(15/7)\langle s^4 \rangle / \langle s^2 \rangle^2$ in homogeneous and isotropic turbulence, where $s^2 = s_{ij} s_{ij}$, $s_{ij} = (\partial u_i/\partial x_j + \partial u_j/\partial x_i)/2$ is the rate-of-strain tensor and we use the summation convention for repeated indices.

Figure 7 shows the flatness factor F in our DNS together with the DNS data by Wang *et al.* (1996) and Gotoh *et al.* (2002), and also DNS and experimental data from figure 6 in Sreenivasan & Antonia (1997). Here time averages taken for the data of Run 2048-2 and Run 4096-2 are also plotted.

Tabeling *et al.* (1996) argued that there is a transition at $R_\lambda \approx 700$ in the dependence of F on R_λ. Such a transition is not seen in our DNS, although our data points are not very dense. The absence of the transition is in agreement with a recent experimental study by Gylfason *et al.* (2004).

The DNS data agree well with the atmospheric measurements of Antonia *et al.* (1981) and are close to the empirical formula

$$F \sim 1.36 R_\lambda^{0.31}, \tag{4.5}$$

used by Hill (2002*a*). They are also close to the recent experimental result

$$F \sim 0.91 R_\lambda^{0.39}, \tag{4.6}$$

of Gylfason *et al.* (2004) for the R_λ range $100 \leqslant R_\lambda \leqslant 1000$.

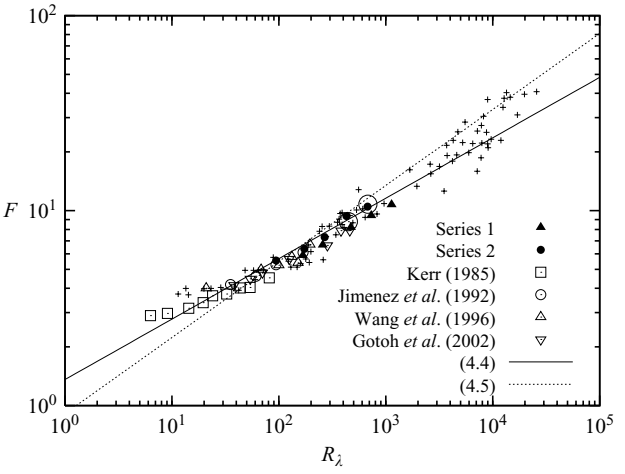

FIGURE 7. Flatness factor F of the longitudinal velocity gradient $\partial u/\partial x$ vs. R_λ. Filled triangles (▲) and circles (●) are the values at $t = t_F$ in Series 1 and 2, respectively; large circles denote the time-averages of $(R_\lambda, -S)$ over t from $t = t_F/2$ to t_F in Run 2048-2 and Run 4096-2. The symbols □, ○, + are from figure 6 in Sreenivasan & Antonia (1997), △ from Wang *et al.* (1996), and ▽ from Gotoh *et al.* (2002); the crosses (+) are from experiments, and the others are from DNS.

A close inspection shows that the DNS data of Series 2 are systematically larger than those of Series 1, and a least-square fitting of the data of Series 2 to $\ln F = \alpha + \beta \ln R_\lambda$ gives

$$F \sim (1.14 \mp 0.19) R_\lambda^{0.34 \pm 0.03}. \tag{4.7}$$

Both (4.5) and (4.6) are not very different from this power law.

4.4. *Fourth-order moments of velocity gradients*

In homogeneous isotropic turbulence, any fourth-order moment of the velocity gradients $g_{ij} \equiv \partial u_i/\partial x_j$ is expressed in terms of the following four rotational invariants (Siggia 1981*b*; Hiero & Dopazo 2003),

$$I_1 \equiv \langle s^4 \rangle, \quad I_2 \equiv \langle s^2 \omega^2 \rangle, \quad I_3 \equiv \langle \omega_i s_{ij} \omega_k s_{kj} \rangle, \quad I_4 \equiv \langle \omega^4 \rangle.$$

If the p.d.f. of g_{ij} were Gaussian, then the normalized invariants defined by

$$F_1 \equiv \frac{15}{7} \frac{I_1}{\langle s^2 \rangle^2} (= F), \quad F_2 \equiv 3 \frac{I_2}{\langle \omega^2 \rangle \langle s^2 \rangle}, \quad F_3 \equiv 3 \frac{I_3}{\langle \omega^2 \rangle \langle s^2 \rangle}, \quad F_4 \equiv \frac{9}{5} \frac{I_4}{\langle \omega^2 \rangle^2},$$

would be 3, 3, 1 and 3, respectively.

Table 2 shows the values of F_1, F_2, F_3 and F_4 from our DNS. In figure 8, we plot them together with the DNS data by Kerr (1985). The DNS data in Series 1 and the time averages in Run 2048-2 and Run 4096-2 are also plotted. It is seen in figure 8 that the values are far from Gaussian and also that inequalities $F_4 > F_2 > F_1 > 3F_3 > 3$ hold for around $R_\lambda > 300$.

The data of Run 512-4 are not plotted in figure 8 because they are almost identical to those of Run 256-2. Table 2 shows that the results of these runs are not very different from each other. This suggests that the results are not sensitive to the wavenumber truncation, k_{max}, provided that $k_{max}\eta \geqslant 2$. (Regarding the possible effects of wavenumber truncation, see, for example, Jiménez *et al.* 1993, Yamazaki, *et al.* 2002, and recent studies by Yakhot & Sreenivasan 2005 and Yeung *et al.* 2006.)

Run	256-1	512-1	1024-1	2048-1	4096-1	256-2	512-2	1024-2	2048-2	4096-2	512-4
R_λ	167	257	471	732	1131	94.3	173	268	429(446)	675(680)	94.6
$-S$	0.505	0.519	0.558	0.579	0.600	0.525	0.544	0.569	0.615(0.602)	0.642(0.648)	0.517
F_1	5.89	6.66	8.20	9.44	10.7	5.55	6.37	7.30	9.37(8.84)	10.5(10.7)	5.42
F_2	6.91	7.86	9.62	11.0	12.4	6.64	7.73	8.86	11.4(10.8)	12.8(13.1)	6.31
F_3	1.02	1.19	1.50	1.77	2.08	0.827	1.02	1.19	1.55(1.45)	1.75(1.79)	0.827
F_4	9.00	10.9	13.3	15.2	17.0	7.92	10.1	11.9	15.7(14.7)	17.7(18.1)	8.04

TABLE 2. DNS values of R_λ, $-S$, F_1, F_2, F_3 and F_4 at $t = t_F$. Time-averages from $t = t_F/2$ to t_F in Run 2048-2 and Run 4096-2 are also shown in parentheses.

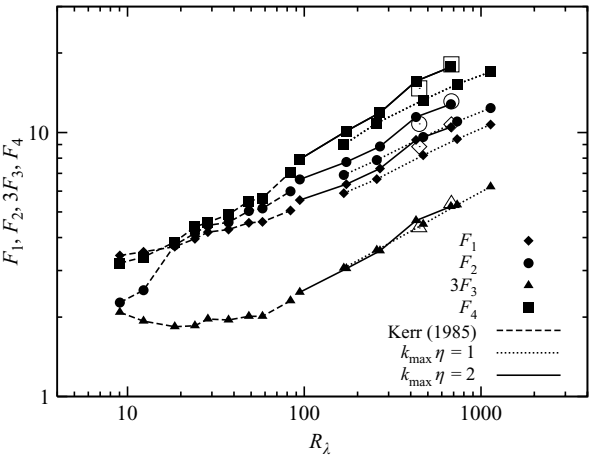

FIGURE 8. F_1, F_2, $3F_3$ and F_4, vs. R_λ at $t = t_F$ in Series 1 and 2. Time averages of F_1, F_2, $3F_3$ and F_4 in Run 2048-2 and Run 4096-2 are plotted by ◇, ○, △, and □, respectively. The dashed lines (- - -) are from Kerr (1985).

By analysing the data of DNS up to $R_\lambda \approx 83$, Kerr (1985) argued that the four invariants I_1, I_2, I_3 and I_4 scale with R_λ differently. On the other hand, by analysing the data of experiments up to $R_\lambda \approx 100$, Zhou & Antonia (2000) argued that they scale similarly.

To see the difference or similarity of the scaling with R_λ of the four rotational invariants, we plot in figures 9(*a*) to 9(*c*) their ratios I_2/I_1, I_3/I_1 and I_4/I_1 from our DNS. The figure suggests the following:

(i) the invariants scale with R_λ differently from each other for around $R_\lambda < 100$, but

(ii) they scale similarly to each other, i.e. the R_λ-dependence of the ratios is weak, for around $R_\lambda > 100$ in Series 2.

The difference of the present observation (ii) from Kerr's is presumably due to the difference in the range of R_λ. Though observation (ii) appears to be in agreement with Zhou & Antonia (2000), it is only for $R_\lambda > 100$, but in Zhou & Antonia (2000), R_λ was up to 100. For $R_\lambda < 100$ in our DNS, they scale differently from each other.

Note also that the slopes of the ratios in Series 1 are slightly different from those in Series 2. The data of Series 1 underestimate the ratios, I_4/I_1, I_2/I_1 and I_1/I_3, compared with those of Series 2, presumably because of insufficient resolution at small scales, as noted at the end of § 4.1. The underestimate of I_4/I_1 in Series 1 together with the inequality $F_4 > F_1$ suggests that the insufficient resolution at small scales has a larger

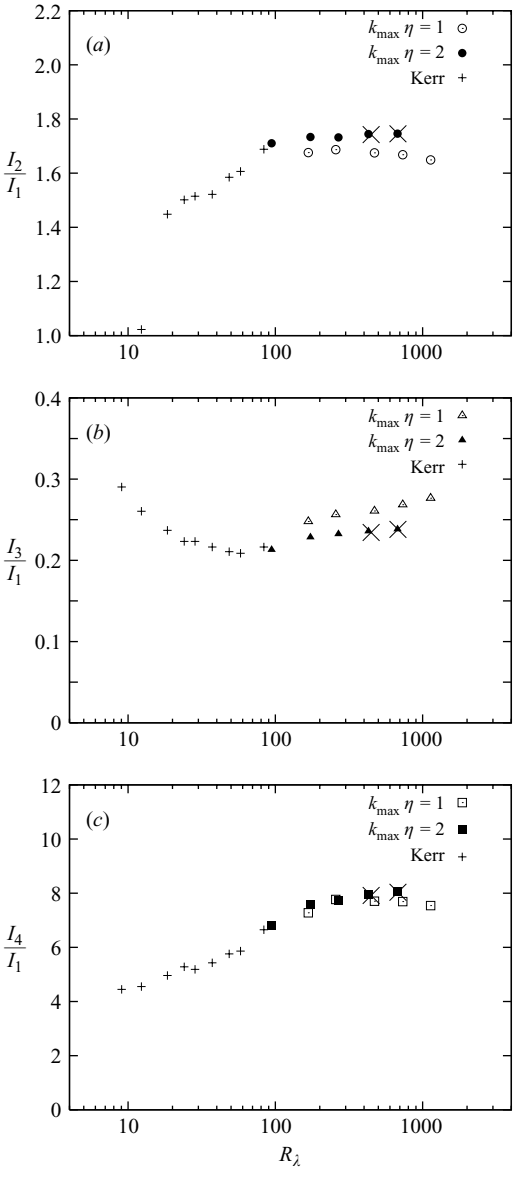

FIGURE 9. Ratios (*a*) I_2/I_1, (*b*) I_3/I_1 and (*c*) I_4/I_1 vs. R_λ at $t = t_F$ in Series 1 and 2. The ratios of time averages of I_1, I_2, I_3 and I_4 in Run2048-2 and Run4096-2 are plotted by $\times$. Data from Kerr (1985) are also plotted by $+$.

effect on I_4 than on I_1. Similarly, the underestimates of I_2/I_1 and I_1/I_3 in Series 1 and the inequalities $F_2 > F_1 > 3F_3$ suggest that the effect of insufficient resolution on I_1 is smaller than that on I_2, but larger than that on I_3.

5. Eulerian and Lagrangian acceleration

The intermittency of turbulence occurs not only in space, but also in time; thus it is seen not only in the velocity gradients, but also in the time derivatives of turbulent velocities.

N	256	512	1024	2048	4096
Series 1	2.85	2.94	2.87	2.82	2.86
Series 2	2.88	2.85	2.92	2.86	2.96

TABLE 3. Flatness of u_i in the runs of Series 1 and 2.

Let us write the NS equation (2.1) symbolically as

$$\boldsymbol{u}^{(1)} \equiv \boldsymbol{a} \equiv \frac{\partial \boldsymbol{u}}{\partial t} = \mathscr{M} : \boldsymbol{u}\boldsymbol{u} + \mathscr{L}\boldsymbol{u}, \tag{5.1}$$

where we have ignored the external force, $\boldsymbol{a}$ is the Eulerian acceleration, and $\mathscr{M} : \boldsymbol{u}\boldsymbol{u}$, and $\mathscr{L}\boldsymbol{u}$ stand for the nonlinear and linear terms in the NS equation (2.1), respectively. Then the Eulerian time derivatives of $\boldsymbol{u}^{(1)} \equiv \boldsymbol{a}$ are as follows:

$$\boldsymbol{u}^{(n+1)} \equiv (\partial/\partial t)^{n+1}\boldsymbol{u} = \sum_{m=0}^{n} {}_nC_m \mathscr{M} : \boldsymbol{u}^{(n-m)}\boldsymbol{u}^{(m)} + \mathscr{L}\boldsymbol{u}^{(n)}, \tag{5.2}$$

where ${}_nC_m = n!/[(n-m)!m!]$.

The Lagrangian time derivative is defined as $\mathrm{D}/\mathrm{D}t \equiv \partial/\partial t + (\boldsymbol{u}\cdot\nabla)$, so that for the Lagrangian acceleration $\boldsymbol{A}$ of a fluid particle (5.1) gives

$$\boldsymbol{A} = \frac{\mathrm{D}\boldsymbol{u}}{\mathrm{D}t} = \left[\frac{\partial}{\partial t} + (\boldsymbol{u}\cdot\nabla)\right]\boldsymbol{u} = \boldsymbol{u}^{(1)} + (\boldsymbol{u}^{(0)}\cdot\nabla)\boldsymbol{u}^{(0)}. \tag{5.3}$$

Similarly, we have

$$\begin{aligned}\frac{\mathrm{D}\boldsymbol{A}}{\mathrm{D}t} &= \frac{\mathrm{D}^2}{\mathrm{D}t^2}\boldsymbol{u} = \left[\frac{\partial}{\partial t} + (\boldsymbol{u}\cdot\nabla)\right]^2 \boldsymbol{u} \\ &= \boldsymbol{u}^{(2)} + (\boldsymbol{u}^{(1)}\cdot\nabla)\boldsymbol{u}^{(0)} + (\boldsymbol{u}^{(0)}\cdot\nabla)\boldsymbol{u}^{(1)} + (\boldsymbol{u}^{(0)}\cdot\nabla)\boldsymbol{A}\end{aligned} \tag{5.4}$$

(see Kaneda, Ishihara & Gotoh 1999, for a systematic derivation of the higher-order time derivatives).

5.1. *Probability distribution functions*

Figure 10 shows the p.d.f.'s of (*a*) the velocity u_i, (*b*) the Eulerian acceleration $a_i = \partial u_i/\partial t$, (*c*) the Lagrangian acceleration $A_i \equiv \mathrm{D}u_i/\mathrm{D}t$, (*d*) the Eulerian time derivative $\partial a_i/\partial t = \partial^2 u_i/\partial t^2$ and (*e*) the Lagrangian derivative $\mathrm{D}A_i/\mathrm{D}t = \mathrm{D}^2 u_i/\mathrm{D}t^2$. We computed the time derivatives using (5.1)–(5.4), in order to avoid errors associated with the time discretization.

It is observed in figure 10(*a*) that the p.d.f.'s of u_i are fairly close to, but not exactly the same as, Gaussian. Table 3 lists the flatness of u_i in the runs of Series 1 and 2 and shows that the flatness of u_i is fairly close, but a little smaller than, Gaussian value 3, in agreement with DNS by Gotoh *et al.* (2002).

Figures 10(*b*) to 10(*e*) show that all the tails of the p.d.f.'s for a_i, $\partial a_i/\partial t$, A_i and $\mathrm{D}A_i/\mathrm{D}t$ are wider for larger R_λ. The comparisons between the p.d.f.'s of $\partial a_i/\partial t = \partial^2 u_i/\partial t^2$ and $a_i \equiv \partial u_i/\partial t$ show that the tails of the p.d.f.'s for $\partial a_i/\partial t = \partial^2 u_i/\partial t^2$ are wider than those for $a_i \equiv \partial u_i/\partial t$, i.e. the former is more intermittent than the latter, as is expected from the fact that the time derivative in (5.1) and (5.2) includes operations that excite high-frequency modes. The same is also true for Lagrangian derivatives; $\mathrm{D}A_i/\mathrm{D}t = \mathrm{D}^2 u_i/\mathrm{D}t^2$ is more intermittent than $A_i \equiv \mathrm{D}u_i/\mathrm{D}t$.

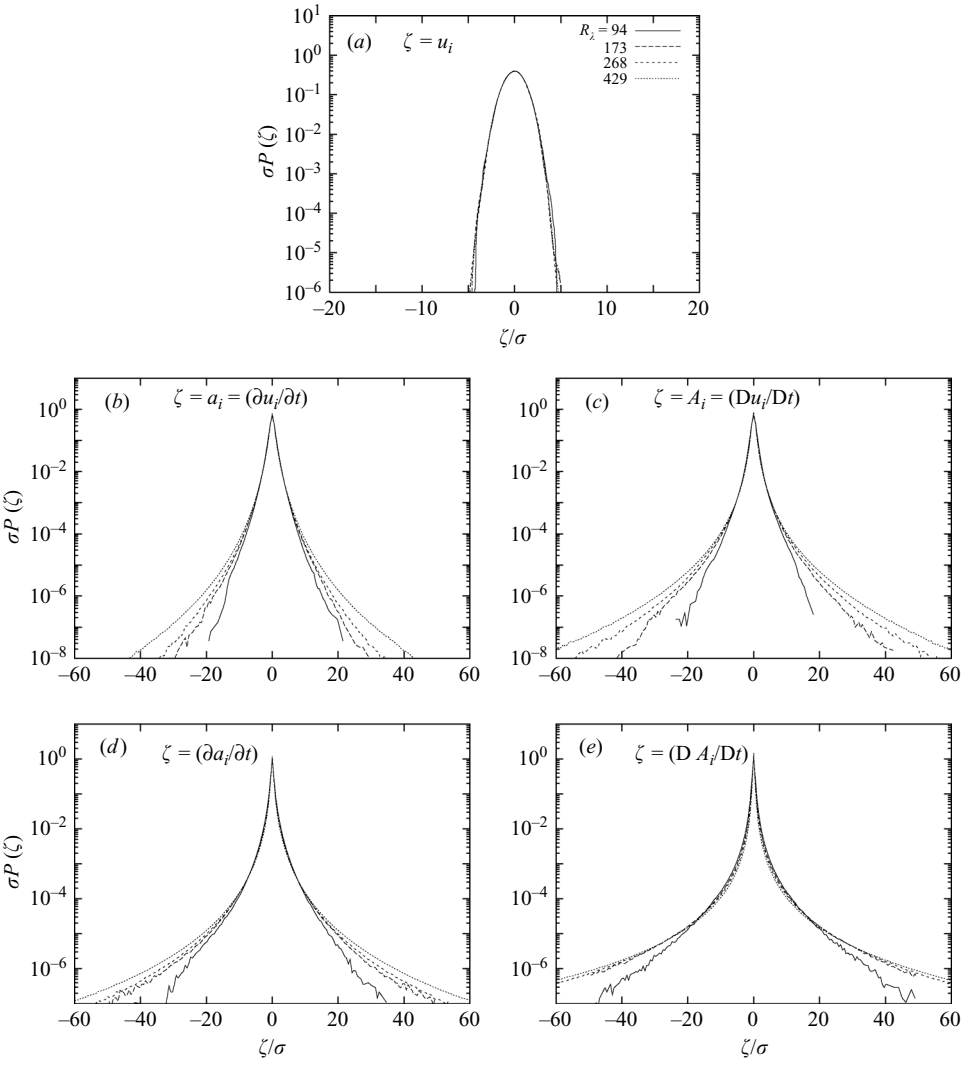

FIGURE 10. P.d.f.'s of (*a*) velocity u_i, (*b*) Eulerian acceleration $a_i = \partial u_i/\partial t$, (*c*) Lagrangian acceleration $A_i = \mathrm{D}u_i/\mathrm{D}t$, (*d*) $\partial a_i/\partial t = \partial^2 u_i/\partial t^2$ and (*e*) $\mathrm{D}A_i/\mathrm{D}t = \mathrm{D}^2 u_i/\mathrm{D}t^2$, normalized by the standard deviations.

The comparisons between figures 10(*b*) and 10(*c*), and between figures 10(*d*) and 10(*e*) show that Lagrangian time derivatives are more intermittent than the Eulerian time derivatives. This is in accordance with the understanding that the Eulerian time-dependence is dominated by the sweeping effect of the energy-containing eddies. Therefore they are less intermittent than the Lagrangian time dependence, which is dominated by interactions among the smaller eddies (e.g. see Kraichnan 1964 and Kaneda *et al.* 1999).

5.2. *Reynolds number dependence of moments*

To quantify the Reynolds number dependence of the p.d.f.'s or the degree of intermittency, we plot the skewness and flatness factors of Eulerian and Lagrangian accelerations in figure 11. The flatness factors are tabulated in table 4. Figure 11(*a*)

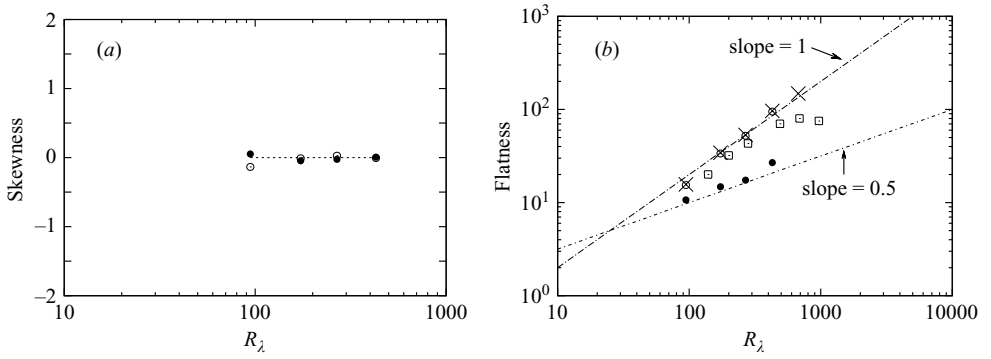

FIGURE 11. (*a*) Skewness of $a_i = \partial u_i/\partial t$ (●) and $A_i = \mathrm{D}u_i/\mathrm{D}t$ (○), and (*b*) flatness factors of a_i (●), A_i (○) and $\partial p/\partial x_i$ (×). Squares (□) are experimental data for A_i by La Porta *et al.* (2001).

Run	256-2	512-2	1024-2	2048-2	4096-2
R_λ	94.3	173	268	429	675
$\langle {a_i}^4\rangle/\langle {a_i}^2\rangle^2$	10.7	14.8	17.4	26.9	—
$\langle {A_i}^4\rangle/\langle {A_i}^2\rangle^2$	15.4(15.7)	33.6(34.3)	52.2(53.2)	94.8(96.5)	—(148)
$\langle {b_i}^4\rangle/\langle {b_i}^2\rangle^2$	52.0	126	183	460	—
$\langle {B_i}^4\rangle/\langle {B_i}^2\rangle^2$	162	705	2460	21345	—

TABLE 4. Flatness factors of the time derivatives of turbulent velocity fields in the runs of Series 2; $a_i = \partial u_i/\partial t$, $A_i = \mathrm{D}u_i/\mathrm{D}t$, $b_i = \partial a_i/\partial t = \partial^2 u_i/\partial t^2$, and $B_i = \mathrm{D}A_i/\mathrm{D}t = \mathrm{D}^2 u_i/\mathrm{D}t^2$. Flatness factor of $\partial p/\partial x_i$ is shown in parentheses for comparison.

shows that the skewness factors of a_i and A_i are almost zero independently of R_λ. This is consistent with the symmetry of the p.d.f.'s of a_i and A_i observed in figure 10(*b*, *c*). Figure 11(*b*) shows that the Lagrangian accelerations are more intermittent than the Eulerian ones, and that

$$\left\langle {a_i}^4\right\rangle \big/ \left\langle {a_i}^2\right\rangle^2 \propto {R_\lambda}^{\alpha_E}, \quad \left\langle {A_i}^4\right\rangle \big/ \left\langle {A_i}^2\right\rangle^2 \propto {R_\lambda}^{\alpha_L}$$

fit well with the DNS, where $\alpha_E \approx 0.5$ and $\alpha_L \approx 1.0$. Figure 11(*b*) also shows that the flatness factor of A_i is almost identical to that of $\partial p/\partial x_i$. A plot (not shown) similar to figure 11(*b*) for $b_i = \partial a_i/\partial t$ and $B_i = \mathrm{D}A_i/\mathrm{D}t$ suggests that

$$\left\langle {b_i}^4\right\rangle \big/ \left\langle {b_i}^2\right\rangle^2 \propto {R_\lambda}^{\beta_E}, \quad \left\langle {B_i}^4\right\rangle \big/ \left\langle {B_i}^2\right\rangle^2 \propto {R_\lambda}^{\beta_L}$$

fit fairly well with the DNS, where $\beta_E \approx 1.5$ and $\beta_L \approx 3.0$.

La Porta *et al.* (2001) measured the fluid particle acceleration experimentally and showed that the acceleration is very intermittent; its flatness factor exceeded 70 for $R_\lambda > 500$. The flatness factor in our DNS is seen in figure 11(*b*) to be close to the experimental values for $R_\lambda < 300$, but it is systematically larger than the experimental values and exceeds 90 even at $R_\lambda = 429$. Recently the flatness factors of A_i were obtained by tracking fluid particles in high-resolution DNS of turbulence (Biferale *et al.* 2005; Yeung *et al.* 2006) and also by processing the Eulerian velocity field in the same way as in this paper (Yeung *et al.* 2006). Our DNS values are systematically larger than the values obtained by tracking fluid particles, especially at high Reynolds

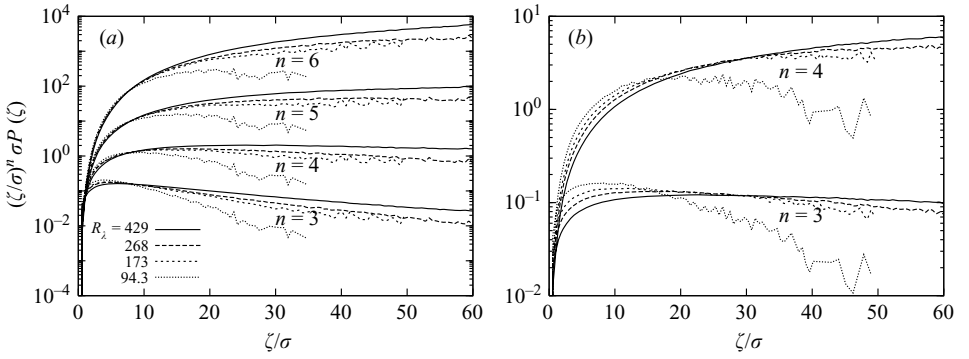

FIGURE 12. Weighted p.d.f. $(\zeta/\sigma)^n \sigma P(\zeta)$ for (*a*) $\zeta = \partial a_i/\partial t$ $(n = 3, 4, 5, 6)$ and (*b*) $\zeta = \mathrm{D}A_i/\mathrm{D}t$ $(n = 3, 4)$, in the runs of Series 2. σ is the standard deviation of ζ.

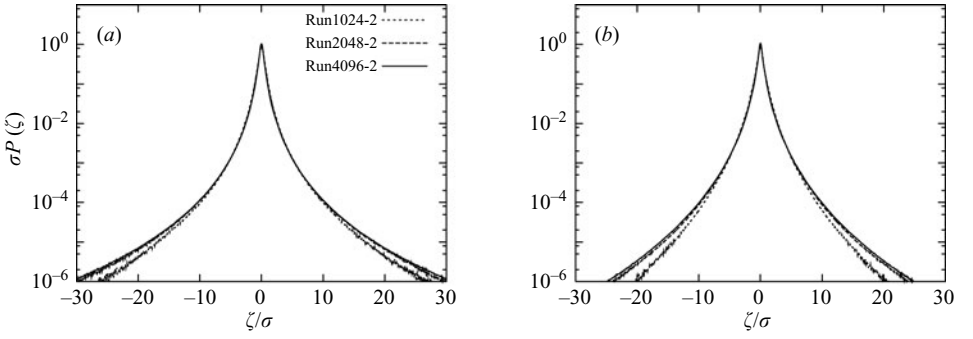

FIGURE 13. P.d.f.'s of (*a*) pressure gradient $\zeta = \partial p/\partial x_i$ and (*b*) viscous term $\zeta = \nu\nabla^2 u_i$. Both $\partial p/\partial x_i$ and $\nu\nabla^2 u_i$ are normalized by the standard deviations.

number. This is consistent with the results in Yeung *et al.* (2006), but the reason remains to be explored.

It is seen in figure 10 that the p.d.f.'s of $\partial a_i/\partial t = \partial^2 u_i/\partial t^2$ and $\mathrm{D}A_i/\mathrm{D}t = \mathrm{D}^2 u_i/\mathrm{D}t^2$ have very wide tails. To see this more clearly, we plot the weighted p.d.f.'s $(\zeta/\sigma)^n \sigma P(\zeta)$ for $\zeta = \partial a_i/\partial t$ $(n = 3, 4, 5, 6)$ and $\zeta = \mathrm{D}A_i/\mathrm{D}t$ $(n = 3, 4)$ in figures 12(*a*) and 12(*b*), respectively, where $\sigma^2 = \langle \zeta^2 \rangle$ and $P(\zeta)$ is the p.d.f. of ζ that gives

$$\langle \zeta^n \rangle = \int_{-\infty}^{\infty} \zeta^n P(\zeta)\, \mathrm{d}\zeta. \tag{5.5}$$

Figures 12(*a*) and 12(*b*) show that $\zeta^n P(\zeta)$ for $\zeta = \partial a_i/\partial t$ $(n = 5, 6)$ and for $\zeta = \mathrm{D}A_i/\mathrm{D}t$ $(n = 4)$ at high R_λ are increasing functions of ζ for at least $\zeta/\sigma < 60$. This shows that $\partial a_i/\partial t$ and $\mathrm{D}A_i/\mathrm{D}t$ are highly intermittent and that the sixth-order moment of $\partial a_i/\partial t$ and the fourth-order moment of $\mathrm{D}A_i/\mathrm{D}t$ at large R_λ are sensitive to very rare events, for which ζ may be as large as $\zeta/\sigma > 60$.

5.3. *Acceleration resulting from the pressure gradient and the viscous drag*

From (5.3), the Lagrangian acceleration A_i of a fluid particle may be written as

$$\boldsymbol{A} = -\nabla p + \nu\nabla^2 \boldsymbol{u}, \tag{5.6}$$

This consists of the acceleration resulting from the pressure gradient and the viscous drag. Figure 13 shows the p.d.f.'s of these two contributions; $\partial p/\partial x_i$ is more intermittent than $\nu\Delta u_i$. This observation is consistent with previous studies (e.g.

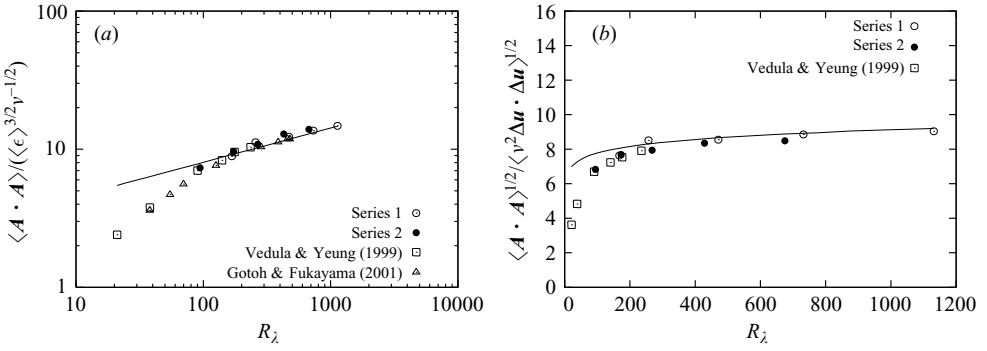

FIGURE 14. (*a*) $\langle \boldsymbol{A} \cdot \boldsymbol{A} \rangle / (\langle \epsilon \rangle^{3/2} \nu^{-1/2})$ vs. R_λ. The solid line is (5.10). (*b*) $\langle \boldsymbol{A} \cdot \boldsymbol{A} \rangle^{1/2} / \{\nu^2 \langle \nabla^2 \boldsymbol{u} \cdot \nabla^2 \boldsymbol{u} \rangle^{1/2}\}$ vs. R_λ. The solid curve is by (5.9) and (5.10).

see Tsinober, Vedula & Yeung 2001). A comparison of the flatness of $\partial p / \partial x_i$ with that of A_i in figure 11(*b*) shows that they are near to each other, though the flatness of $\partial p / \partial x_i$ is slightly larger than that of A_i.

For incompressible homogeneous turbulence $\langle \nabla p \cdot \boldsymbol{u} \rangle = 0$, so that (5.6) gives

$$\langle \boldsymbol{A} \cdot \boldsymbol{A} \rangle = \langle \nabla p \cdot \nabla p \rangle + \langle \nu^2 \nabla^2 \boldsymbol{u} \cdot \nabla^2 \boldsymbol{u} \rangle . \tag{5.7}$$

Figures 14(*a*) and 14(*b*) show the DNS values of $\langle \boldsymbol{A} \cdot \boldsymbol{A} \rangle$ normalized by $\langle \epsilon \rangle^{3/2} \nu^{-1/2}$ and the square root of the ratio of $\langle \boldsymbol{A} \cdot \boldsymbol{A} \rangle / \langle \nu^2 \nabla^2 \boldsymbol{u} \cdot \nabla^2 \boldsymbol{u} \rangle$, respectively. The DNS values by Vedula & Yeung (1999) and Gotoh & Fukayama (2001), which are in good agreement with the present DNS, are also included in the figures. No systematic dependence of the normalized values of $\langle \boldsymbol{A} \cdot \boldsymbol{A} \rangle$ on $k_{\max} \eta$ is seen. Figure 14(*b*) shows that $\nu^2 \langle \nabla^2 \boldsymbol{u} \cdot \nabla^2 \boldsymbol{u} \rangle^{1/2}$ is much less than $\langle \boldsymbol{A} \cdot \boldsymbol{A} \rangle^{1/2}$; the ratio of the former to the latter ranges from 1/8 to 1/10 for $300 < R_\lambda < 1200$.

By surveying the existing DNS and experimental data, Hill (2002*a*) proposed the following empirical formula for the covariances in (5.7) at $R_\lambda > 400$:

$$\langle \nabla p \cdot \nabla p \rangle / \left(\langle \epsilon \rangle^{3/2} \nu^{-1/2} \right) \sim 3.1 H_\chi F^{0.79} \sim 3.9 H_\chi R_\lambda^{0.25} \sim 2.5 R_\lambda^{0.25}, \tag{5.8}$$

$$\langle \nu^2 \nabla^2 \boldsymbol{u} \cdot \nabla^2 \boldsymbol{u} \rangle / \left(\langle \epsilon \rangle^{3/2} \nu^{-1/2} \right) = \frac{35}{2} 15^{-3/2} \, |S| \sim 0.08 R_\lambda^{0.11}, \tag{5.9}$$

and

$$\langle \boldsymbol{A} \cdot \boldsymbol{A} \rangle / \left(\langle \epsilon \rangle^{3/2} \nu^{-1/2} \right) \sim 2.5 R_\lambda^{0.25} + 0.08 R_\lambda^{0.11}, \tag{5.10}$$

for homogeneous and isotropic turbulence. Figure 14 shows that the DNS data fit well with these formulae.

In (5.8), H_χ is a constant defined by

$$H_\chi = \langle \nabla p \cdot \nabla p \rangle / \left(4 \int_0^\infty r^{-3} D_{1111}(r) \, \mathrm{d}r \right), \tag{5.11}$$

in which $D_{1111}(r)$ is the fourth-order velocity structure function defined by $D_{1111}(r) = \langle (u_1(\boldsymbol{x} + \boldsymbol{r}) - u_1(\boldsymbol{x}))^4 \rangle$, and u_1 is a velocity component parallel to the separation vector $\boldsymbol{r}$. Vedula & Yeung (1999) measured the values of H_χ at $R_\lambda < 240$ using DNS of turbulence and found that the values approach an asymptotic value of about 0.65. In figure 15, we plot the values of H_χ in our DNS; the values are estimated from the DNS data for $\langle \nabla p \cdot \nabla p \rangle$ and $D_{1111}(r)$. The figure shows that the

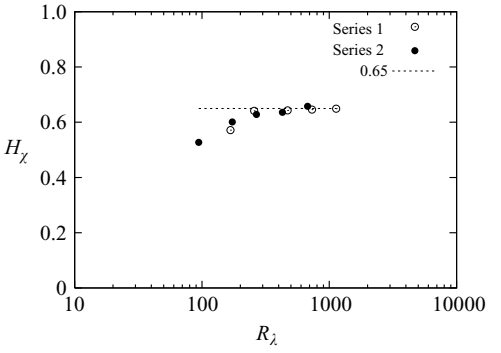

FIGURE 15. R_λ dependence of H_χ.

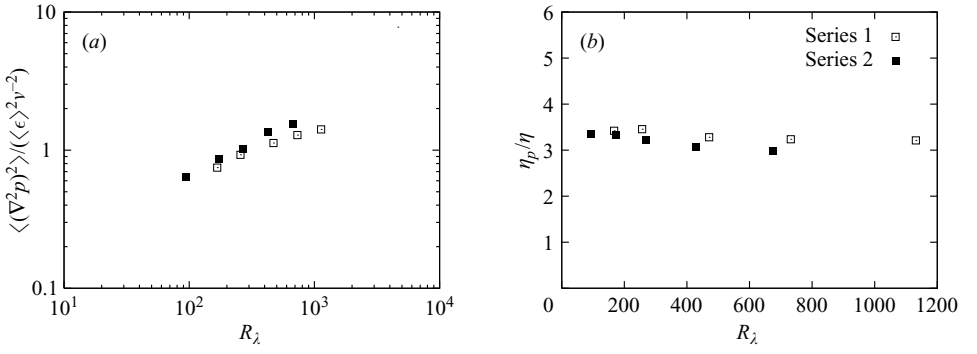

FIGURE 16. (*a*) $\langle(\nabla^2 p)^2\rangle$ normalized by $\langle\epsilon\rangle^2\nu^{-2}$ and (*b*) the ratio $\eta_p/\eta = \left[\langle\nabla p\cdot\nabla p\rangle/\langle(\nabla^2 p)^2\rangle\right]^{1/2}/\eta$ vs. R_λ.

values of H_χ are insensitive to $k_{\max}\eta$ and suggests that H_χ approaches a constant (approximately 0.65) for large R_λ.

The comparison of the covariances $\langle\nabla p\cdot\nabla p\rangle$ and $\langle(\nabla^2 p)^2\rangle$ yields a length scale η_p such that

$$\eta_p^2 \equiv \frac{\langle\nabla p\cdot\nabla p\rangle}{\langle(\nabla^2 p)^2\rangle}.$$

In the theory of anomalous scaling of structure functions proposed by Yakhot (2003), the assumption that η_p and η have similar scaling with respect to R_λ plays a key role. It may therefore be of interest to examine this with the DNS data. Figure 16 shows DNS data for the covariance $\langle\epsilon\rangle^{3/2}\nu^{-1/2}$ and the ratio η_p/η: the dependence of the ratio on R_λ is weak at large R_λ, and the data of Series 2 (Series 1) gives the estimate $\eta_p/\eta \sim 3.0(3.2)$ at large R_λ. Note that the small scale is not very well resolved in Series 1.

6. Spectral analysis

6.1. *Skewness*

Some idea of the dependence of S on R_λ discussed in § 4.1 may be obtained by using $k^2 T(k) = 2\nu k^4 E(k)$, which holds in the wavenumber range where the external force is negligible in statistically stationary homogeneous isotropic turbulence. This equality

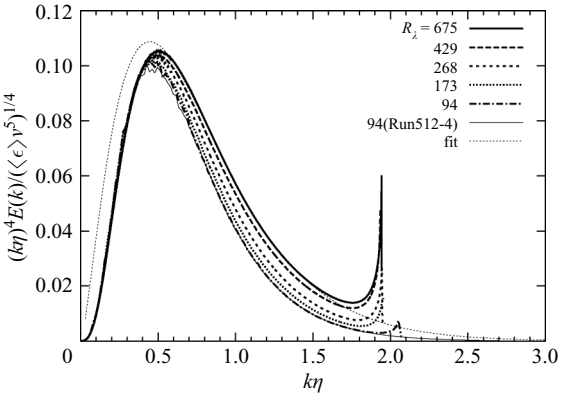

FIGURE 17. Normalized spectrum $k^4E(k)$ vs. $x = k\eta$ in the DNS of Series 2. The spectrum at $t = t_F$ of DNS with $R_\lambda = 94$, $N = 512$, $k_{max}\eta \approx 4$ (Run 512-4) and a fitting function to the data for $0.5 < k\eta < 1.5$ of Run 4096-2 are also plotted.

enables us to rewrite (4.1) as

$$-S \sim \frac{4}{35} 15^{3/2} \int_0^\infty x^4 f(x)\,\mathrm{d}x, \tag{6.1}$$

where $f(k\eta) \equiv E(k)/(\langle\epsilon\rangle\nu^5)^{1/4}$ and $x \equiv k\eta$.

Figure 17 shows the integrand $x^4 f(x)$ in (6.1) for various R_λ in Series 2. It is seen that

(i) the integral in (6.1) is dominated by the contribution from the near dissipation range ($x = k\eta \approx 1$),

(ii) $x^4 f(x)$ is insensitive to R_λ at $x < 0.5$, but

(iii) it is not as insensitive to R_λ at $0.5 < x (< 2.0)$ and

(iv) $x^4 f(x)$ is larger for the larger R_λ at $0.5 < x$.

These facts imply that S may be sensitive to the R_λ dependence of the spectrum $E(k)$ in the near dissipation range $x \approx 0.5$. The observation (iv) is consistent with the increase of $-S$ with R_λ as seen in figure 6.

A recent DNS analysis by Ishihara *et al.* (2005) suggests that $f(x)$ in the near dissipation range $x \approx 1$ fits well with $F(x) = Cx^\alpha \exp(-\beta x)$, where C, α, β are constants independent of x. By comparing the energy spectrum in Run 256-2 with that in Run 512-4, they confirmed that

(i) there is no significant difference in $f(x)$ between these two runs in the wavenumber range $x < 1.7$, and

(ii) the function $F(x)$ fits well with the DNS data of $f(x)$ not only in the range $x \approx 1$, but also up to $x \approx 4$.

The results (i) and (ii) encourage us to use an approximation such as

$$\int_0^\infty x^4 f(x)\,\mathrm{d}x = \int_0^{0.5} x^4 f(x)\,\mathrm{d}x + \int_{0.5}^\infty C x^{\alpha+4} \exp(-\beta x)\,\mathrm{d}x, \tag{6.2}$$

in which $f(x)$, C, α and β are estimated from the data of the DNS with $k_{max}\eta \approx 2$. We confirmed that the value of S computed by (6.2) is close to the one by (3.2) or (4.1). For example, the difference is only approximately 0.5% in Run 4096-2.

According to the analysis by Ishihara *et al.* (2005), as $R_\lambda \to \infty$, then C, α, β approach constants independent of R_λ in agreement with Kolmogorov, but the approach is very slow. This implies that (i) the observed dependence of S on R_λ may be attributed to

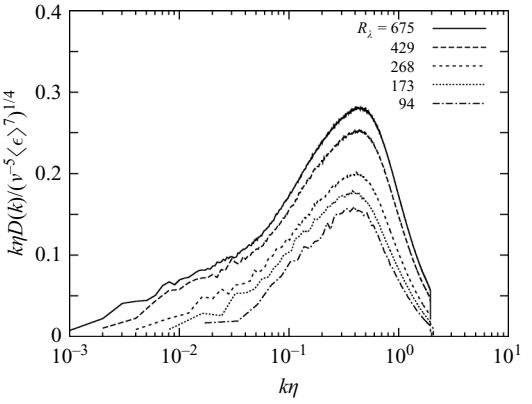

FIGURE 18. $k\eta D(k)/(\nu^{-5}\langle\epsilon\rangle^7)^{1/4}$ at $t = t_F$ in Series 2.

the dependence of these constants on R_λ at finite R_λ, and (ii) as $R_\lambda \to \infty$, S approaches a constant independent of R_λ, but the approach may be very slow.

6.2. *Flatness factor of the longitudinal velocity gradient*

Let $D(k)$ be the spectrum of $\langle s^4 \rangle$ such that $\langle s^4 \rangle = \int_0^\infty D(k)\,\mathrm{d}k$. Then

$$F = \frac{15}{7}\int_0^\infty \tilde{D}(x)\,\mathrm{d}x, \tag{6.3}$$

where $\tilde{D}(k\eta) = D(k)/(\nu^{-5}\langle\epsilon\rangle^7)^{1/4}$, and $x = k\eta$. Figure 18 show the spectrum $x\tilde{D}(x)$ at $t = t_F$ in Series 2. Since $\tilde{D}(x)\mathrm{d}x = x\tilde{D}(x)\,\mathrm{d}(\ln x)$, the height of $x\tilde{D}(x)$ in the figure is proportional to the contribution to the integral (6.3) from the range $(\ln x, \ln x + \mathrm{d}[\ln x])$.

Note that to rigorously evaluate $D(k)$ from $\hat{\boldsymbol{u}}(\boldsymbol{k})$ ($|\boldsymbol{k}| \leqslant k_{\max}$), one has to perform a fast Fourier transform of s^2 with $N/2 > 2k_{\max}$ because $\widehat{s^2}(\boldsymbol{k})$ has non-zero modes for $|\boldsymbol{k}| < 2k_{\max}$. Here we do not perform such a costly computation, so that $\int_0^{k_{\max}} D(k)\,\mathrm{d}k$ does not exactly give $\langle s^4 \rangle$. However in our computation of $D(k)$, the alias error in computing $\widehat{s^2}(\boldsymbol{k})$ was removed as in Ishihara *et al.* (2003), so that $D(k)$ for $k < k_{\max}$ is free from any alias error, and therefore has no artificial peak at the highest available mode, in contrast to $k^4E(k)$.

It is observed from figure 18 that

(i) the dominant contribution to the integral (6.3) comes from the near dissipation range $0.1 < x < 1$, but

(ii) there is a substantial contribution not only from the near dissipation range, but also from the range $x < 0.1$,

(iii) $x\tilde{D}(x)$ increase with R_λ at all x, and

(iv) the relative contribution from $x < 0.1$ to the integral increases with R_λ.

Observation (iii) is consistent with the increase of F with R_λ. Observations (ii) and (iv) imply that not only the dissipation range, but also the range $x < 0.1$ is responsible for the R_λ-dependence of F.

6.3. *Fourth-order moments of velocity gradients*

Let $W(k)$ and $\Omega(k)$ be the spectra of $\langle s_{ij}\omega_j s_{im}\omega_m \rangle$ and $\langle(\omega^2/2)^2\rangle$, respectively. Then F_3 and F_4 can be expressed in the forms

$$F_3 = \frac{3}{2}\int_0^\infty \tilde{W}(x)\,\mathrm{d}x, \quad F_4 = \frac{9}{5}\int_0^\infty \tilde{\Omega}(x)\,\mathrm{d}x, \tag{6.4}$$

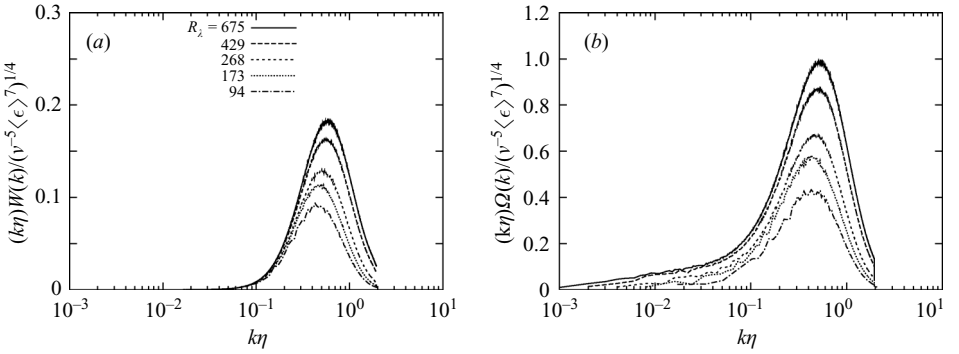

FIGURE 19. (*a*) $k\eta W(k)/(\nu^{-5}\langle\epsilon\rangle^7)^{1/4}$ and (*b*) $k\eta\Omega(k)/(\nu^{-5}\langle\epsilon\rangle^7)^{1/4}$ at $t = t_F$ in Series 2.

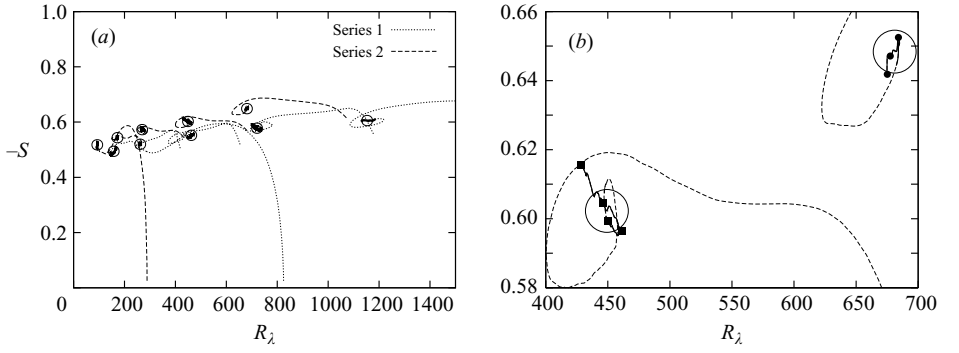

FIGURE 20. (*a*) Trajectories in the $(-S, R_\lambda)$-plane from $t = 0$ to $t = t_F$. Solid lines are the trajectory from $t = t_F/2$ to $t = t_F$. Circles are the averages over t from $t = t_F/2$ to $t = t_F$ in each run. (*b*) A close-up view of (*a*) for the trajectories in Run2048-2 and Run 4096-2. Filled squares are the points at $t = 5.2$, 6.8, 8.4 and 10 in Run 2048-2, and filled circles $t = 2.6$, 3.2 and 3.8 in Run 4096-2.

respectively, where $x = k\eta$. Figures 19(*a*) and 19(*b*) show the spectra $x\tilde{W}(x)$ and $x\tilde{\Omega}(x)$, respectively, at various R_λ. It is seen that

(i) there is no substantial contribution to F_3 from the range $x < 0.1$ (figure 19*a*),

(ii) the dominant contribution to the integral of F_4 is from the near dissipation range ($x \approx 0.5$), but

(iii) there is a non-negligible contribution to F_4 not only from the range $x > 0.1$, but also from $x < 0.1$ (figure 19*b*), as with $F_1 = F$.

It was shown in Ishihara *et al.* (2003) that $\tilde{D}(x) \sim \tilde{\Omega}(x)$ at $x < 0.1$, but $\tilde{D}(x) \ll \tilde{\Omega}(x)$ at $x > 0.1$, as is confirmed by figures 18 and 19(*c*). This implies that the relative influence on F_4 from the range $x < 0.1$, which is determined by $\tilde{\Omega}(x)$, compared with that from $x > 0.1$ is weaker than that on F_1.

7. Discussion

7.1. *Mutual relations between one-point statistics of velocity gradients*

The analyses in §4 show that the DNS data fit well with the simple power-law dependence of S, F_1, F_2, F_3 and F_4 on R_λ. However, a close inspection of instantaneous statistics at various times reveals that the dependence may be not as simple in a strict sense. This is demonstrated by figures 20(*a*) and 20(*b*). The former shows the

N	256	512	1024	2048	4096
Series 1	0.494 ± 0.010	0.520 ± 0.002	0.552 ± 0.005	0.578 ± 0.007	0.605 ± 0.002
Series 2	0.518 ± 0.008	0.544 ± 0.004	0.573 ± 0.005	0.602 ± 0.006	0.648 ± 0.003

TABLE 5. Time average and the standard deviation of $-S$ from $t_F/2$ to t_F

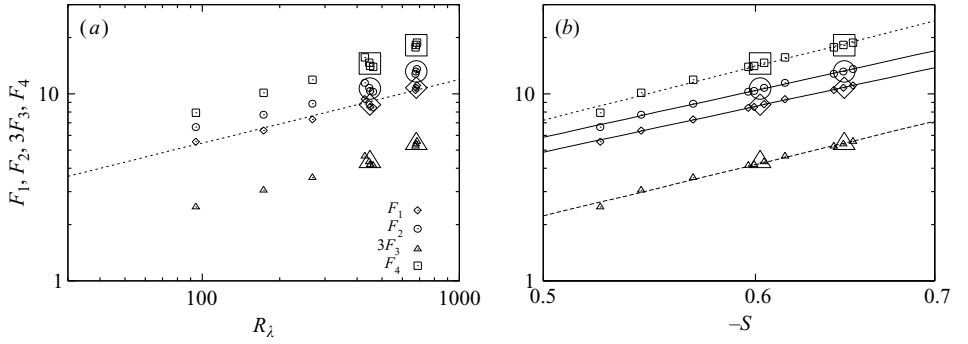

FIGURE 21. (*a*) DNS values of F_1, F_2, $3F_3$ and F_4 vs. R_λ at $t = t_F$ in Series 2. DNS values at $t = 5.2$, 6.8 and 8.4 in Run 2048-2 and those at $t = 2.6$ and 3.2 in Run 4096-2 are also plotted. Time averages for Run 2048-2 and Run 4096-2 are shown by large symbols. The straight line is (4.7). (*b*) The data in (*a*) are plotted against $-S$. The straight lines are (7.1).

trajectories of runs in Series 2 in the $(R_\lambda, -S)$-plane, and the latter shows a close-up view of the trajectories for Run 2048-2 and Run 4096-2. It might appear from figure 20(*a*) that after a transient period, the trajectory of each run converges to a point, while figure 20(*b*) shows that the trajectory continues to move in a complicated way even after the transient period. Regarding the latter, however, the standard deviation of the values of $-S$ over the interval from $t = t_F/2$ to t_F in each run is not large and at most a few percent of the mean, as seen in table 5.

The time averages of R_λ and $-S$ over the interval from $t = t_F/2$ to t_F in each run are plotted in the $(R_\lambda, -S)$-plane in figure 20(*a*, *b*), showing that

(i) the instantaneous values of $-S$ in each run have a complex R_λ-dependence, even in the quasi-stationary state after the transient period, but

(ii) the time average of $-S$ (circles), in contrast to the instantaneous value, has a simpler R_λ-dependence.

Figure 21(*a*) plots the values of F_1, F_2, F_3 and F_4 as a function of R_λ, and figure 21(*b*) plots them as a function of $-S$, in which we plot not only time averages, but also instantaneous values at various times for Run 2048-2 and Run 4096-2. Figure 21(*a*) shows that

(iii) the instantaneous values of F_1, F_2, F_3 and F_4 depend on R_λ in a complicated way, and

(iv) their dependences on R_λ and time correlate well with each other.

Figure 21(*b*) shows

(v) not only the time averages, but also the instantaneous values of F_1, F_2, F_3 and F_4 have a much simpler dependence on S than on R_λ.

A least-square fitting of the data in figure 21(*b*) to $\ln F_n = \alpha_n + \beta_n \ln(-S)$ gives

$$F_n \sim C_n(-S)^{\beta_n} \quad (n = 1, 2, 3, 4), \tag{7.1}$$

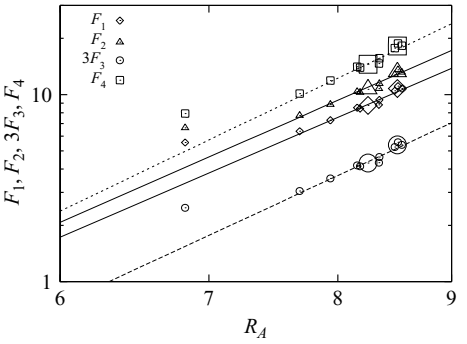

FIGURE 22. The data in figure 21 are plotted against R_A. The straight lines are the least square fits to the instantaneous data for $R_A > 7.5$.

where $\ln C_n = \alpha_n$ and

$$(C_1, \beta_1) = (41.5 \mp 0.8, 3.09 \pm 0.04), \quad (C_2, \beta_2) = (52.4 \mp 1.3, 3.16 \pm 0.05),$$
$$(C_3, \beta_3) = (8.2 \mp 0.4, 3.46 \pm 0.09), \quad (C_4, \beta_4) = (90 \mp 6, 3.6 \pm 0.1).$$

The power law $F_1 \sim 41.5(-S)^{3.09}$ is consistent with the relation between F and S obtained from (4.4) and (4.7). However, note that the deviation of the data from the power laws is much less in figure 21(b) than in figures 6 and 7.

7.2. *Reynolds number based on Lagrangian acceleration*

Hill (2002*b*) proposed the Reynolds numbers R_A and $R_{\nabla p}$ defined by

$$R_A = \langle \boldsymbol{A} \cdot \boldsymbol{A} \rangle^{1/2} / \langle \nu^2 \nabla^2 \boldsymbol{u} \cdot \nabla^2 \boldsymbol{u} \rangle^{1/2},$$
$$R_{\nabla p} = \langle \nabla p \cdot \nabla p \rangle^{1/2} / \langle \nu^2 \nabla^2 \boldsymbol{u} \cdot \nabla^2 \boldsymbol{u} \rangle^{1/2},$$

respectively, and argued that

$$R_A \sim R_{\nabla p} \sim (2.0 F^{0.79} / 0.3|S|)^{1/2}, \tag{7.2}$$

which is obtained using (5.9), (5.9) and $H_\chi \approx 0.65$, may be related to F by a power law, provided that S is related to F by a power law.

Figure 22 gives the DNS values of $F_1 (= F)$, F_2, $3F_3$ and F_4 as a function of R_A. It shows that

(i) DNS values of the four rotational invariants are related well to R_A by power laws for $R_A > 7.5$ or so, but

(ii) the deviations of the instantaneous values from the power laws are not as small as those in figure 21(b).

Figure 21(b) has suggested that not only the time-averaged values, but also the instantaneous values of the four rotational invariants are related well to $-S$ by power laws. Figures 22 and 21(b) show that regarding the instantaneous values, the relation between $-S$ and the invariants is simpler than that between R_A and the invariants.

Note that

$$\begin{pmatrix} -S \\ F_1 \\ F_3 \\ F_4 \end{pmatrix} \propto \int \begin{pmatrix} k^5 E(k) \\ kD(k) \\ kW(k) \\ k\Omega(k) \end{pmatrix} \mathrm{d}(\ln k),$$

while

$$\begin{pmatrix} \langle \nabla p \cdot \nabla p \rangle \\ \langle (\nabla^2 p)^2 \rangle \end{pmatrix} = \int \begin{pmatrix} k^3 P(k) \\ k^5 P(k) \end{pmatrix} \mathrm{d}(\ln k).$$

An inspection of the spectra shows that $k^5 E(k)$, $kD(k)$, $kW(k)$, $k\Omega(k)$ and $k^5 P(k)$ as a function of $\ln(k\eta)$ have their peaks at $k\eta \approx 0.6$, but $k^3 P(k)$ has its peak at $k\eta \approx 0.25$. This implies that the dominant contribution to $-S$, F_1, F_3, F_4 and $\langle (\nabla^2 p)^2 \rangle$ comes from the near dissipation range, but that to $\langle \nabla p \cdot \nabla p \rangle$ it is from the wavenumber range slightly lower than the near dissipation range.

8. Conclusions

In this paper we have studied one-point statistics of velocity gradients and Eulerian and Lagrangian accelerations on the basis of the data from high-resolution DNS of turbulence with the number of grid points up to 4096^3 and R_λ up to 1130 (Series 1) or 675 (Series 2). To obtain a better understanding of the relation between the one-point statistics, we used not only the instantaneous statistics at $t = t_\mathrm{F}$, but also time averages over the time interval from $t = t_\mathrm{F}/2$ to t_F in Run 2048-2 and Run 4096-2 in § 4.

Particular attention was paid to the possible dependence of the statistics on the Reynolds number Re. As quantitative measures of the Re dependence of the p.d.f.'s of the velocity gradients, we considered the skewness and flatness factors of the gradients. The DNS data show that the skewness S and flatness factors F of the longitudinal velocity gradients fit well with power laws

$$S \sim -(0.32 \mp 0.02) R_\lambda^{0.11 \pm 0.01} \text{ and } F \sim (1.14 \mp 0.19) R_\lambda^{0.34 \pm 0.03}.$$

This power-law dependence on R_λ is consistent with previous experimental studies (Sreenivasan & Antonia 1997; Gylfason *et al.* 2004). No transition in the R_λ dependence of S at $R_\lambda \approx 700$ is visible in our DNS, in contrast to Tabeling *et al.* (1996).

The observed dependences of the skewness and flatness factors on Re or R_λ imply that the p.d.f.'s are also Re dependent. Their power law dependences imply that within the Re-range we studied, the DNS do not support the conjecture that the p.d.f.'s tend to certain universal forms independent of Re with the increase of Re.

The DNS values of normalized rotational invariants $F_n (n = 1, 2, 3, 4)$ proposed by Siggia (1981*b*) are far from the Gaussian values and increase with R_λ. The DNS data suggest that for $R_\lambda > 100$, in contrast to $R_\lambda < 83$ reported by Kerr (1985), all of the invariants scale with R_λ similarly to each other.

In a strict sense, turbulence characteristics including R_λ, $\langle \epsilon \rangle$, S and L fluctuate in time even in the quasi-stationary state after the transient period. As a consequence, the normalized invariants, F_n, also fluctuate in time to some extent. A close inspection suggests that the time dependences of the F_n are similar to each other and correlate better with S than with R_λ.

We have also analysed the statistics of accelerations. It was confirmed that for both the Eulerian and Lagrangian velocities, the second-order time derivatives are more intermittent than the first-order derivatives and that the Lagrangian time derivatives of turbulent velocities are more intermittent than the Eulerian time derivatives, as would be expected. The flatness factors of the Eulerian and Lagrangian accelerations increase with R_λ as $\propto R_\lambda^{\alpha_E}$ and $\propto R_\lambda^{\alpha_L}$, respectively, where $\alpha_E \approx 0.5$ and $\alpha_L \approx 1.0$. The flatness factor of the Lagrangian acceleration is >90 at $R_\lambda \approx 430$. The DNS data show that the second-order Eulerian and Lagrangian time derivatives of the velocity

are highly intermittent and that their flatness factors increase with R_λ as proportional to $R_\lambda^{\beta_E}$ and $R_\lambda^{\beta_L}$, respectively, where $\beta_E \approx 1.5$ and $\beta_L \approx 3.0$.

The spectral analysis presented in § 6.1 suggests that the observed dependence of S on R_λ may be attributed to the dependence of the energy spectrum on R_λ at finite R_λ and that, as $R_\lambda \to \infty$, S approaches a constant independent of R_λ, but the approach may be slow.

S, $F_1(=F)$, F_3 and F_4 can be expressed as integrals of normalized spectra with respect to $x \equiv k\eta$ from $x = 0$ to ∞. The dominant contribution to any of these integrals is mainly from the near dissipation range. However, there is substantial contribution to F_1 and F_4 not only from the range $x > 0.1$, but also from $x < 0.1$. These results imply that S, $F_1(=F)$, F_3 and F_4 are mainly dominated by the small-scale statistics of turbulence, but the statistics of eddies with sizes larger than around 10η also have a non-negligible influence on F_1 and F_4, i.e. F_1 and F_4 are more sensitive to the large-scale structure of turbulence than S and F_3 are. Since the influence from the range $x < 0.1$ on F_1 as compared with that from $x > 0.1$ is stronger than that on F_4 (Ishihara *et al.* 2003), F_1 is expected to be more sensitive to the large-scale structure of turbulence than F_4.

The computations were carried out on the Earth Simulator at Japan Agency for Marine–Earth Science and Technology and on the HPC2500 system at the Information Technology Center of Nagoya University. This work was supported by Grant-in-Aids for Scientific Research (B)17340117, (C)17560051 and (C)19560064, from the Japan Society for the Promotion of Science, and also by a Grant-in-Aid for the 21st COE program "Frontiers of Computational Science".

REFERENCES

Antonia, R., Chambers, A. & Satyaprakash, B. 1981 Reynolds number dependence of high-order moments of the streamwise turbulent velocity derivative. *Boundary Layer Met.* **21**, 159–171.

Belin, F., Maurer, J., Tabeling, P. & Willaime, H. 1997 Velocity gradient distribution in fully developed turbulence: An experimental study. *Phys. Fluids* **9**, 3843–3850.

Biferale, L., Boffetta, G., Celani, A., Devenish, B. J., Lanotte, A. & Toschi, F. 2004 Multifractal statistics of Lagrangian velocity and acceleration in turbulence. *Phys. Rev. Lett.* **93**, 064502.

Biferale, L., Boffetta, G., Celani, A., Lanotte, A. & Toschi, F. 2005 Particle trapping in three-dimensional fully developed turbulence. *Phys. Fluids* **17**, 021701.

Champagne, F. H. 1978 The fine-scale structure of the turbulent velocity field. *J. Fluid Mech.* **86**, 67–108.

Gotoh, T. & Fukayama, D. 2001 Pressure spectrum in homogeneous turbulence. *Phys. Rev. Lett.* **86**, 3775–3779.

Gotoh, T., Fukayama, D. & Nakano, T. 2002 Velocity field statistics in homogeneous steady turbulence obtained using a high-resolution direct numerical simulation. *Phys. Fluids* **14**, 1065–1081.

Gotoh, T. & Rogallo, R. S. 1999 Intermittency and scaling of pressure at small scales in forced isotropic turbulence. *J. Fluid Mech.* **396**, 257–285.

Gylfason, A., Ayyalasomayajula, S. & Warhaft, Z. 2004 Intermittency, pressure and acceleration statistics from hot-wire measurements in wind-tunnel turbulence. *J. Fluid Mech.* **501**, 213–229.

Hierro, J. & Dopazo, C. 2003 Fourth-order statistical moments of the velocity gradient tensor in homogeneous, isotropic turbulence. *Phys. Fluids* **15**, 3434–3442.

Hill, R. J. 2002*a* Scaling of acceleration in locally isotropic turbulence. *J. Fluid Mech.* **452**, 361–370.

Hill, R. J. 2002*b* Possible alternative to R_λ-scaling of small-scale turbulence statistics. *J. Fluid Mech.* **463**, 403–412.

Ishihara, T. & Kaneda, Y. 2002 High resolution DNS of incompressible homogeneous forced turbulence – Time dependence of the statistics. In *Proc. Intl Workshop on Statistical Theories and Computational Approaches to Turbulence* (ed. Y. Kaneda & T. Gotoh), pp. 179–188. Springer.

Ishihara, T., Kaneda, Y., Yokokawa, M., Itakura, K. & Uno, A. 2003 Spectra of energy dissipation, enstrophy and pressure by high-resolution direct numerical simulations of turbulence in a periodic box. *J. Phys. Soc. Japan* **72** 983–986.

Ishihara, T., Kaneda, Y., Yokokawa, M., Itakura, K. & Uno, A. 2005 Energy spectrum in the near dissipation range of high resolution direct numerical simulation of turbulence. *J. Phys. Soc. Japan* **74** 1464–1471.

Jiménez, J., Wray, A. A., Saffman, P. G. & Rogallo, R. S. 1993 The structure of intense vorticity in isotropic turbulence. *J. Fluid Mech.* **255**, 65–90.

Kaneda, Y. & Ishihara, T. 2006 High-resolution direct numerical simulation of turbulence. *J. Turbulence* **7**, 20.

Kaneda, Y., Ishihara, T. & Gotoh, K. 1999 Taylor expansions in powers of time of Lagrangian and Eulerian two-point two-time velocity correlations in turbulence. *Phys. Fluids* **11**, 2154–2166.

Kaneda, Y., Ishihara, T., Yokokawa, M., Itakura, K. & Uno, A. 2003 Energy dissipation rate and energy spectrum in high resolution direct numerical simulations of turbulence in a periodic box. *Phys. Fluids* **15**, L21–L24.

Kerr, R. M. 1985 Higher-order derivative correlations and the alignment of small-scale structures in isotropic numerical turbulence. *J. Fluid Mech.* **153**, 31–58.

Kolmogorov, A. N. 1941 The local structure of turbulence in incompressible viscous fluid for very large Reynolds number. *C. R. Acad. Sci. URSS* **30**, 299–303.

Kraichnan, R. H. 1964 Kolmogorov hypotheses and Eulerian turbulence theory, *Phys. Fluids.* **7**, 1723–1734.

La Porta, A., Voth, G. A., Crawford, A. M., Alexander, J. & Bodenschatz, E. 2001 Fluid particle accelerations in fully developed turbulence. *Nature* **409**, 1017–1019.

Sawford, B. L., Yeung, P. K., Borgas, M. S., La Porta, A., Crawford, A. M. & Bodenschatz, E. 2003 Conditional and unconditional acceleration statistics in turbulence. *Phys. Fluids* **15**, 3478–3489.

Siggia, E. D. 1981*a* Numerical study of small-scale intermittency in three-dimensional turbulence. *J. Fluid Mech.* **107**, 375–406.

Siggia, E. D. 1981*b* Invariants for the one-point vorticity and strain rate correlation functions *Phys. Fluids* **24**, 1934–1936.

Sreenivasan, K. R. & Antonia, R. A. 1997 The phenomenology of small-scale turbulence. *Annu. Rev. Fluid Mech.* **29**, 435–472.

Tabeling, P., Zocchi, G., Belin, F., Maurer, J. & Willaime, H. 1996 Probability density functions, skewness, and flatness in large Reynolds number turbulence. *Phys. Rev.* E **53**, 1613–1621.

Tsinober, A., Vedula, P. & Yeung, P. K. 2001 Random Taylor hypothesis and the behavior of local and convective accelerations in isotropic turbulence. *Phys. Fluids* **13**, 1974–1984.

Vedula, P. & Yeung, P. K. 1999 Similarity scaling of acceleration and pressure statistics in numerical simulations of isotropic turbulence. *Phys. Fluids* **11**, 1208–1220.

Vincent, A. & Meneguzzi, M. 1991 The spatial structure and statistical properties of homogeneous turbulence. *J. Fluid Mech.* **225**, 1–20.

Wang, L.-P., Chen, S., Brasseur, J. G. & Wyngaard, J. C. 1996 Examination of hypotheses in the Kolmogorov refined turbulence theory through high-resolution simulations. Part 1. Velocity field. *J. Fluid Mech.* **309**, 113–156.

Yakhot, V. 2003 Pressure-velocity correlations and scaling exponents in turbulence. *J. Fluid Mech.* **495**, 135–143.

Yakhot, V. & Sreenivasan, K. R. 2005 Anomalous scaling of structure functions and dynamic constraints on turbulence simulations. *J. Statist Phys.* **121**, 823–841.

Yamazaki, Y., Ishihara, T. & Kaneda, Y. 2002 Effects of wavenumber truncation on high-resolution direct numerical simulation of turbulence *J. Phys. Soc. Japan* **71**(3), 771–781.

Yeung, P. K. 2002 Lagrangian investigations of turbulence. *Annu. Rev. Fluid Mech.* **34**, 115–142.

Yeung, P. K., Pope, S. B., Lamorgese, A. G. & Donzis, D. A. 2006 Acceleration and dissipation statistics of numerically simulated isotropic turbulence. *Phys. Fluids* **18**, 065103-1-14.

Yokokawa, M., Itakura, K., Uno, A., Ishihara, T. & Kaneda, Y. 2002 16.4-Tflops direct numerical simulation of turbulence by a Fourier spectral method on the Earth Simulator Proceeding of the IEEE/ACM SC2002 Conference (CD-ROM), Baltimore. (http://www.sc-2002.org/paperp.d.f.s/pap.pap273.pdf).

Zhou, T. & Antonia, R. A. 2000 Reynolds number dependence of the small-scale structure of grid turbulence *J. Fluid Mech.* **406**, 81–107.